Award Number: W81XWH-08-1-0765

TITLE: Consortium for Bone and Tissue Repair and Regeneration

PRINCIPAL INVESTIGATOR: J. David Eick, Ph.D.

CONTRACTING ORGANIZATION: University of Missouri
Kansas City MO 64108

REPORT DATE: October 2009

TYPE OF REPORT: Annual

PREPARED FOR: U.S. Army Medical Research and Materiel Command
Fort Detrick, Maryland 21702-5012

DISTRIBUTION STATEMENT:)

■ Approved for public release; distribution unlimited

The views, opinions and/or findings contained in this report are those of the author(s) and should not be construed as an official Department of the Army position, policy or decision unless so designated by other documentation.

REPORT DOCUMENTATION PAGE

Form Approved
OMB No. 0704-0188

Public reporting burden for this collection of information is estimated to average 1 hour per response, including the time for reviewing instructions, searching existing data sources, gathering and maintaining the data needed, and completing and reviewing this collection of information. Send comments regarding this burden estimate or any other aspect of this collection of information, including suggestions for reducing this burden to Department of Defense, Washington Headquarters Services, Directorate for Information Operations and Reports (0704-0188), 1215 Jefferson Davis Highway, Suite 1204, Arlington, VA 22202-4302. Respondents should be aware that notwithstanding any other provision of law, no person shall be subject to any penalty for failing to comply with a collection of information if it does not display a currently valid OMB control number. **PLEASE DO NOT RETURN YOUR FORM TO THE ABOVE ADDRESS.**

1. REPORT DATE *(DD-MM-YYYY)*	2. REPORT TYPE	3. DATES COVERED *(From - To)*
01-10-2009	Annual	26 Sep 2008 - 25 Sep 2009

4. TITLE AND SUBTITLE

*Consortium for bone and tissue repair and regeneration

5a. CONTRACT NUMBER

5b. GRANT NUMBER
W81XWH-08-1-0765

5c. PROGRAM ELEMENT NUMBER

6. AUTHOR(S)

J. David Eick, Ph.D.
Email: eickj@umkc.edu

5d. PROJECT NUMBER

5e. TASK NUMBER

5f. WORK UNIT NUMBER

7. PERFORMING ORGANIZATION NAME(S) AND ADDRESS(ES)

University of Missouri
5100 Rockhill Road
Kansas City MO 64108

8. PERFORMING ORGANIZATION REPORT NUMBER

9. SPONSORING / MONITORING AGENCY NAME(S) AND ADDRESS(ES)

U.S. Army Medical Research and Materiel Command
Ft. Detrick, MD 21701

10. SPONSOR/MONITOR'S ACRONYM(S)

11. SPONSOR/MONITOR'S REPORT NUMBER(S)

12. DISTRIBUTION / AVAILABILITY STATEMENT

Distribution is unlimited.

13. SUPPLEMENTARY NOTES

14. Abstract - see next page

14. ABSTRACT

Building upon the considerable strengths of the University of Missouri-Kansas City (UMKC) in biomaterials, biological systems, and clinical expertise and Missouri University of Science and Technology (Missouri S&T) in biomaterials, materials science and engineering, and the engineering disciplines, the Consortium provides a seamless mechanism for designing and developing new biomaterials far exceeding the capacity of the individual groups at each campus. The development of new biomaterials is a joint effort, bringing together life scientists and materials engineers in the development and testing of new biomaterials. The Consortium focuses on the following:

- Speeding up the development of new materials for the repair and regeneration of traumatized bone and tissues by establishing an efficient, shared infrastructure for biomaterials, biosensors, and bio-interfacial research.
- Promoting interdisciplinary collaboration that enhances the rate of scientific discovery and technological advances to develop the next generation of biomaterials and biosensors.
- Developing joint programs to train the next generation of biomedical and biomaterials engineers, providing a future workforce for the US Army and the vital US biotechnology industry.
- Promoting technology transfer and entrepreneurship to commercialize new knowledge, which will improve patient outcomes while expanding economic development in Missouri and the nation.

The proposed project is a collaborative research effort by faculty at UMKC and Missouri S&T for the purpose of creating three-dimensional (3-D) scaffolds composed of bioactive glass fibers, micro-spheres, and particles whose unique structure and properties are optimized for the repair and regeneration of diseased or damaged bones in humans. In addition to being designed to be bioactive and reacting in a biologically beneficial manner with tissue fluids, these 3-D scaffolds will also (1) provide surface features such as high surface area nanostructured hydroxyapatite (HA) that promote cell attachment and proliferation, (2) contain nano- and micro-sized pores conducive to cell growth and function, and (3) release trace elements and protein growth factors that are known to be biologically important to the development of healthy bone. The design, fabrication, and property evaluation of these unique 3-D scaffolds is the primary responsibility of the Missouri S&T faculty participants, with the UMKC faculty providing significant input in the desired biological performance.

The UMKC faculty bears primary responsibility for evaluating and validating the biological performance of the scaffolds in vitro and in vivo and determining how the viability, attachment, proliferation, and differentiation of bone cells is affected by the structural features and chemical properties of a given scaffold. This collaborative work is expected to yield scaffolds that will eventually be evaluated in human experiments, with emphasis on limb and craniofacial applications. Hypothesis: A bioactive 3-D glass scaffold can be developed by the Consortium which will be superior to currently available bone grafting materials and will meet a need of the US Army for advanced biomaterials to repair and regenerate traumatized bone.

KEY RESEARCH ACCOMPLISHMENTS

- Prepared three candidate bioactive glasses with silicate (13-93), borosilicate (13-93B1), and borate (13-93B3) composition, as well as the widely studied silicate 45S5 glass (control);
- Converted three glasses (13-93; 13-93B1; 13-93B3) into porous three-dimensional scaffolds with two different microstructures (described as 'fibrous' and 'trabecular');
- Evaluated the in vitro bioactivity (conversion to a hydroxyapatite-type material in a simulated body fluid) and mechanical response of 13-93, 13-93B1, and 13-93B3 bioactive glass scaffolds with fibrous and trabecular microstructures;
- Evaluated in vitro response of MLO-A5 cells (an established osteogenic cell line) to scaffolds of 13-93 bioactive glass with fibrous and trabecular microstructures;
- Evaluated in vitro response of MLO-A5 cells to bioactive glasses and glass scaffolds of three different compositions (13-93, 13-93B1, and 13-93B3);
- Evaluated the ability of 13-93, 13-93B1, and 13-93B3 bioactive glass scaffolds with the fibrous and trabecular microstructures to support tissue infiltration in a subcutaneous rat implantation model;
- Initiated in vivo experiments: implantation of 13-93 and 13-93B3 scaffolds in dorsal skinfold chambers in rats to assess possible angiogenic responses;
- Initiated in vitro tests of covalently bonding a bioadhesive peptide to 13-93 glass scaffolds as a means of enhancing the attachment, growth, and function of osteogenic cells;
- Prepared scaffolds for implantation into rat calvaria defect model in Year 2, and imaged the scaffolds using microCT on the day of implantation.

15. SUBJECT TERMS

None provided.

16. SECURITY CLASSIFICATION OF:			**17. LIMITATION OF ABSTRACT**	**18. NUMBER OF PAGES**	**19a. NAME OF RESPONSIBLE PERSON**
a. REPORT	**b. ABSTRACT**	**c. THIS PAGE**			**19b. TELEPHONE NUMBER** *(include area code)*
U	U	U	UU	27	

Table of Contents

Page

INTRODUCTION

Building upon the strengths of Missouri University of Science and Technology (Missouri S&T) and the University of Missouri-Kansas City (UMKC), the Consortium was formed to design and develop unique bioactive glass scaffolds which will meet a need of the US Army for advanced biomaterials to repair and regenerate traumatized bone. The **hypothesis** of the research is that three-dimensional bioactive glass scaffolds can be developed by the Consortium which will be superior to currently available bone grafting materials. In addition to being designed to be bioactive and reacting in a biologically beneficial manner with tissue fluids, these scaffolds will also (1) provide surface features such as high surface area nanostructured hydroxyapatite (HA) that promote cell attachment and proliferation, (2) contain nano- and micro-sized pores conducive to cell growth and function, and (3) release trace elements and protein growth factors that are known to be biologically important to the development of healthy bone. This collaborative effort is expected to yield scaffolds that will eventually be evaluated in human experiments, with emphasis on limb and craniofacial applications.

BODY

The research accomplishments associated with the tasks/objectives for Year 1 (Phase I) of the project are described in the following sections.

Objective A: Preparation of Bioactive Glasses (Missouri S&T)

Four glasses, designated 45S5, 13-93, 13-93B1, and 13-93B3, with the compositions given in Table 1 were prepared by conventional glass melting and casting procedures, as described in our previous work (Huang et al., 2006). Glass rods (~10 mm in diameter) were formed by casting the molten glass in steel dies. These rods were sliced with a low-speed diamond saw to produce discs (1 mm thick) to be used in subsequent cell culture studies. Short fibers and particles of the glasses were formed for subsequent preparation of porous scaffolds. The molten glass was first quenched on stainless steel plates. Fibers were prepared by re-melting the glass for 1 h at 1200°C–1400°C, drawing fibers (diameter = 100–300 μm) from the melt, and chopping the fibers to a length of 3 ± 1 mm). Particles (<5–10 μm) were prepared by crushing the quenched glass in a hardened steel mortar and pestle, sieving through stainless steel sieves to give particles <150 μm, and attrition milling for 2 h (**Fig. 1**).

Table 2. Nominal composition (in wt%) of bioactive glasses used in this project.

Glass	SiO_2	B_2O_3	Na_2O	K_2O	MgO	CaO	P_2O_5
45S5	45.0	-	24.5	-	-	24.5	6.0
13-93	53.0	-	6.0	12.0	5.0	20	4.0
13-93B1	34.4	20.0	5.8	11.6	4.9	19.5	3.9
13-93B3	0	56.6	5.5	11.1	4.6	18.5	3.7

Objective B: As-prepared Glass Surface vs. Pre-reacted (Incubated) Surface (UMKC)

Discs of 45S5, 13-93, 13-93B1, and 13-93B3 (prepared in Objective A) were sterilized with 70% ethanol for 1 hr, air dried, and then coated with collagen for 1 hr before air drying. The bioactive glass discs were tested with and without pre-incubation in media to determine if pre-reaction in culture media would have an effect on bone cell proliferation. The cells were plated on the discs at 3.5×10^4 cells/well using alpha MEM/5%FBS/5%CS. Cells plated on the plastic surface were used as a positive control. After 24 and 48 hrs, the media was removed and the cells released with trypsin/EDTA and counted using a Coulter Counter. The results are shown in **Fig. 1**. With no pre-incubation (**Fig. 1a**), essentially no toxicity was observed with 45S5 as expected, nor with 13-93 or 13-93B1. However 13-93B3 was toxic, most likely due to the increased percentage of borate. With 4 hrs pre-incubation in culture media, the toxicity of 13-93B3 was reduced, but still evident at 48 hrs (**Fig. 1b**). Experiments were performed to determine the effects of the bioactive glasses on a marker of osteoblast differentiation and function, alkaline phosphatase enzyme activity (**Fig. 2**). The 13-93 and 13-93B1 were similar if not slightly better than the 45S5, but the 13-93B3 had toxic effects on the cells.

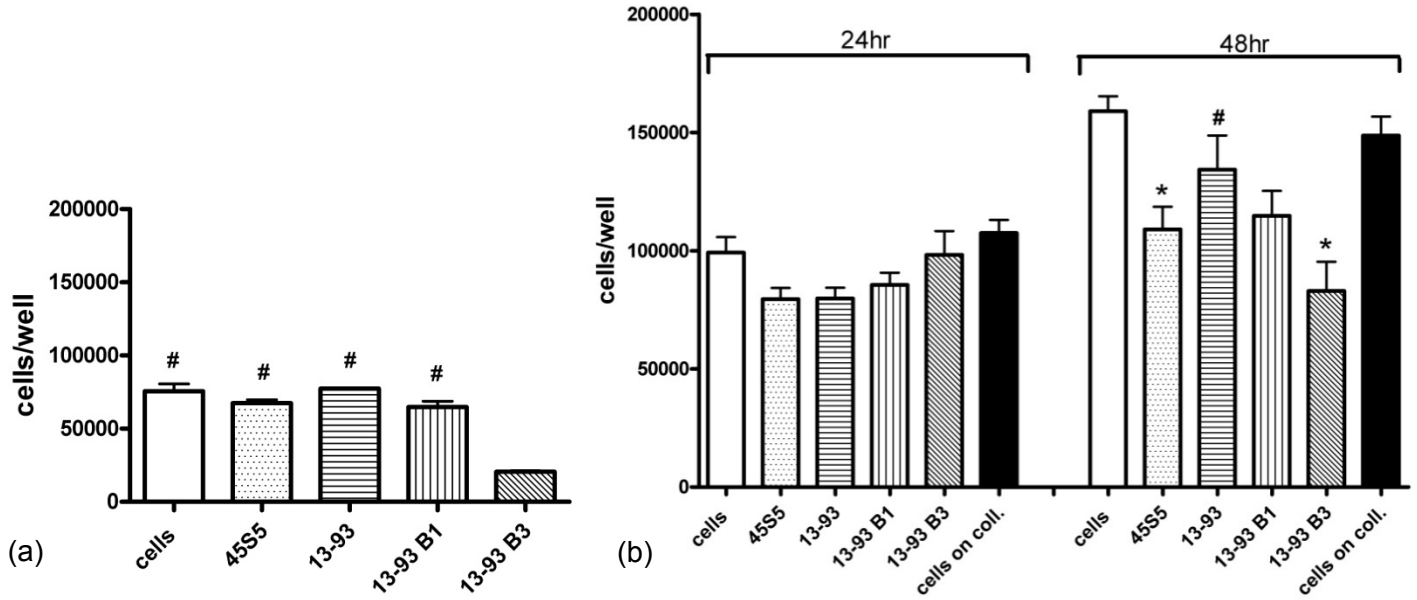

Fig. 1. Effects of silicate 45S5, silicate 13-93, borosilicate 13-93B1, and borate 13-93B3 glass on proliferation of MLO-A5 bone cells. (a) Cells cultured for 24 h on disks without pre-incubation, (n=3) and (b) for 24 and 48 h with pre-incubation for 4 h in media (n=4). Cells plated on plastic control wells (denoted cells) or cells on collagen were used as controls. (n=3) # $p<0.001$ compared to 13-93B3 for (A). *$p<0.05$ compared to cells, # $p<0.05$ compared to 13-93B3 for (B). Significance based on OneWay ANOVA, followed by Tukey post-test. (Bonewald, UMKC).

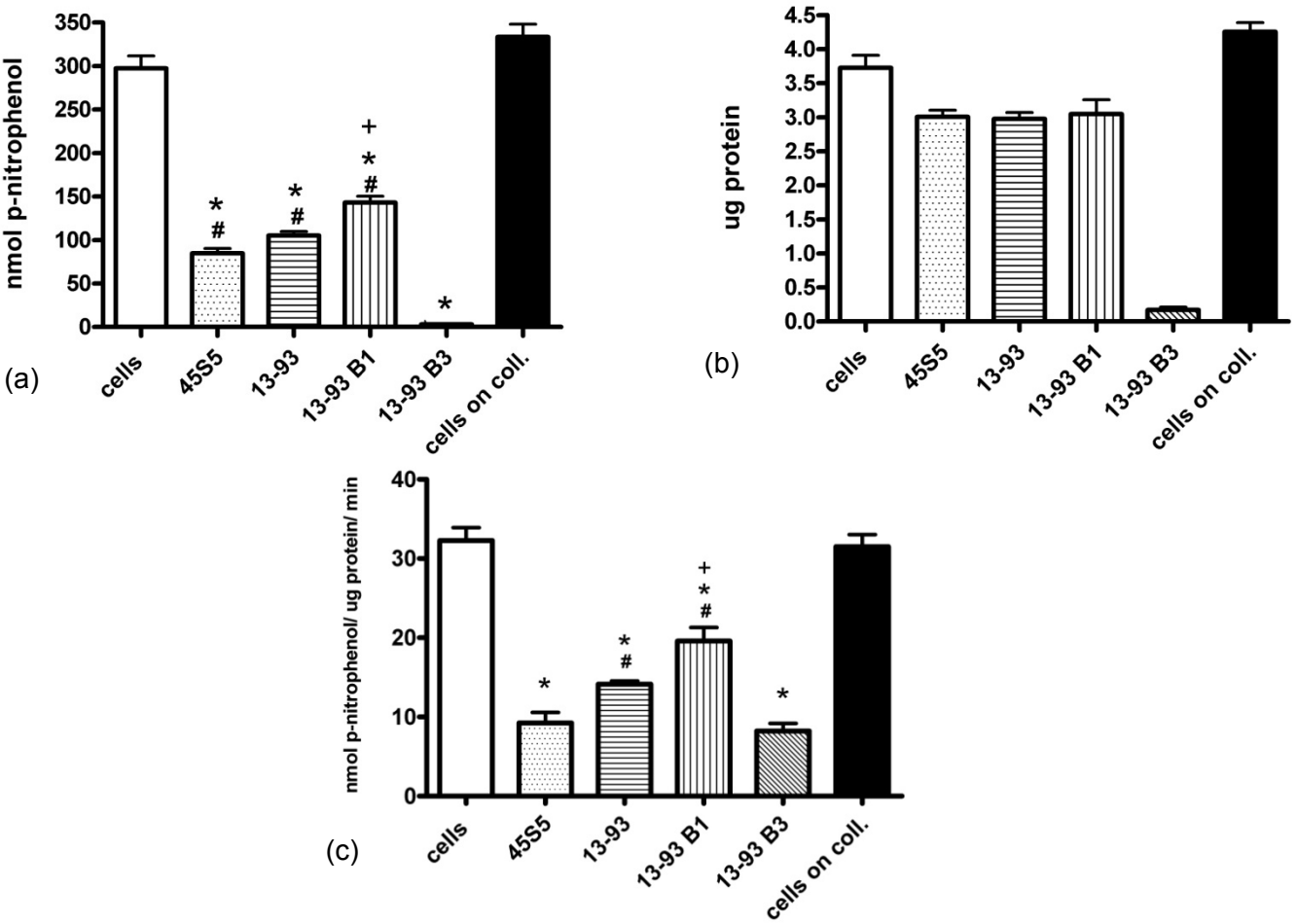

Fig. 2. Effects of 45S5, 13-93, 13-93B1, and 13-93B3 glass on alkaline phosphatase enzyme activity at day 4 of culture of MLO-A5 cells. (a) Enzyme activity in nmole p-nitrophenol activity, $p<0.01$ compared to 45S5, *$p<0.001$ compared to cells, # $p<0.001$ compared to 13-93B3), (b) Protein and (c) enzyme specific activity (+$p<0.001$ compared to 45S5,

*p<0.001 compared to cells, # p<0.05 compared to 13-93B3, p<0.05 of 13-93 vs. 13-91B1). Cells plated on plastic control wells (denoted cells) or cells on collagen were used as controls. (n=4). (Bonewald, UMKC).

Objective C: Preparation of Scaffolds (Missouri S&T)

Porous three-dimensional scaffolds of each glass (45S5, 13-93, 13-93B1, and 13-93B3) with two different microstructures, referred to as 'trabecular' and 'fibrous', were prepared at Missouri S&T.

Trabecular scaffolds: Trabecular scaffolds, with a microstructure similar to that of dry human trabecular bone, were prepared using a polymer foam replication technique, as described in detail elsewhere (Fu et al., 2008). Briefly, a commercial polyurethane foam with the requisite pore structure was infiltrated with a stabilized slurry (suspension) of glass particles (prepared in Objective A). After drying, the particle-coated foams were subjected to a controlled heat treatment to first decompose the foam and then sinter the glass into a dense network. The heating schedule was 1°C/min to 500°C in O_2 gas, then 5°C/min to the sintering temperature: 1 h at 700°C for 13-93, 630°C for 13-93B1, and 570°C for 13-93B3. Trabecular scaffolds of 45S5 glass prepared using this method crystallized during sintering, which limited the sintering of the glass particles, resulting in scaffolds with low strength. **Figure 3** shows scanning electron microscope (SEM) images of the 13-93, 13-93B1, and 13-93B3 scaffolds with the trabecular microstructure. The scaffolds had open porosity of 75–85%, as determined using the Archimedes method, and pores sizes in the range 100–500 μm, as determined using mercury porosimetry. These pore characteristics satisfy the requirements (open porosity >50–60%; mean pore size >100–150 μm) which are considered to be favorable to permit tissue ingrowth and function in porous scaffolds.

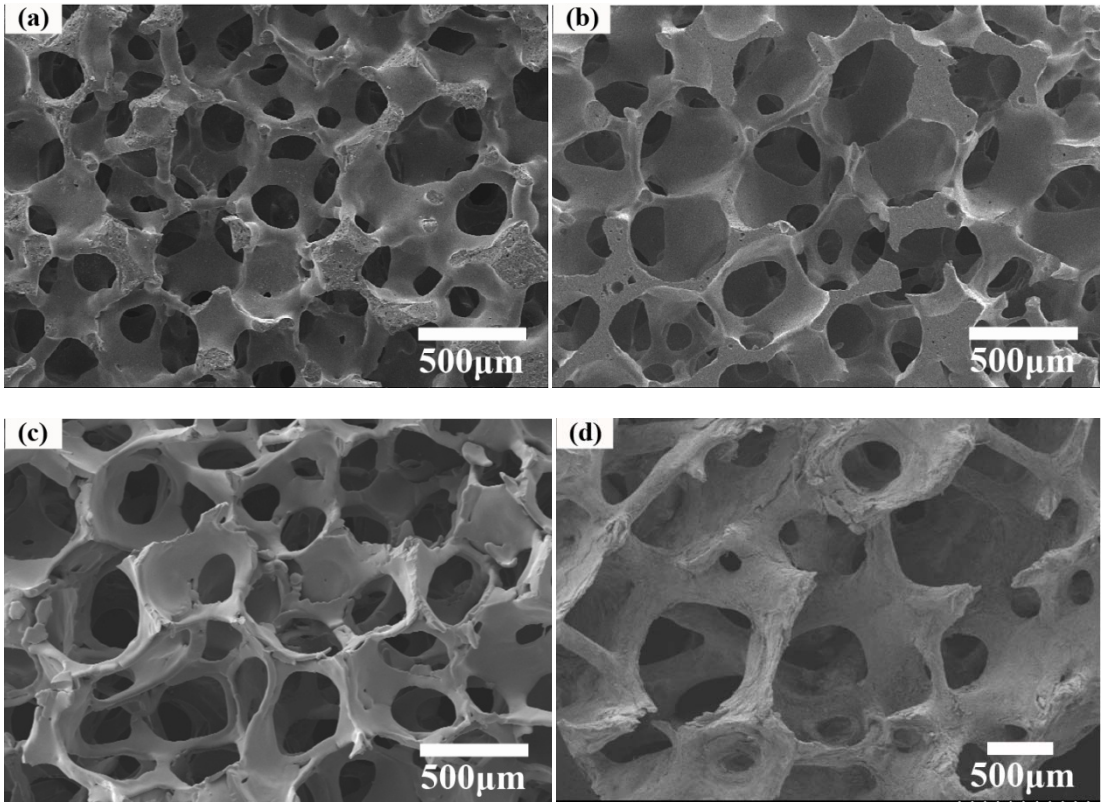

Fig. 3. SEM images of (a) 13-93, (b) 13-93B1, and (c) 13-93B3 bioactive glass scaffolds prepared by the polymer foam replication method. (d) SEM image of a dry human trabecular bone is shown for comparison. (Rahaman, Missouri S&T).

Bioactivity of scaffolds: The bioactivity of the trabecular scaffolds was evaluated by measuring their rate of conversion to a hydroxyapatite-type material in a simulated body fluid (SBF) at 37°C. The composition of the SBF was identical to that described by Kokubo et al. (1990). The conversion reaction is accompanied by a weight loss of the scaffolds, as well as a change in pH value of the SBF, so the kinetics of conversion were determined by measuring these two quantities as a function of time. For both the fibrous and trabecular scaffolds, the glass composition had a marked effect on their *in vitro* bioactivity (**Fig. 4**). The weight loss of the

scaffolds increased with increasing B_2O_3 content of the glass (**Fig. 4a**). Concurrently, the pH of the SBF also increased markedly with the B_2O_3 content of the scaffold (Fig. **4b**).

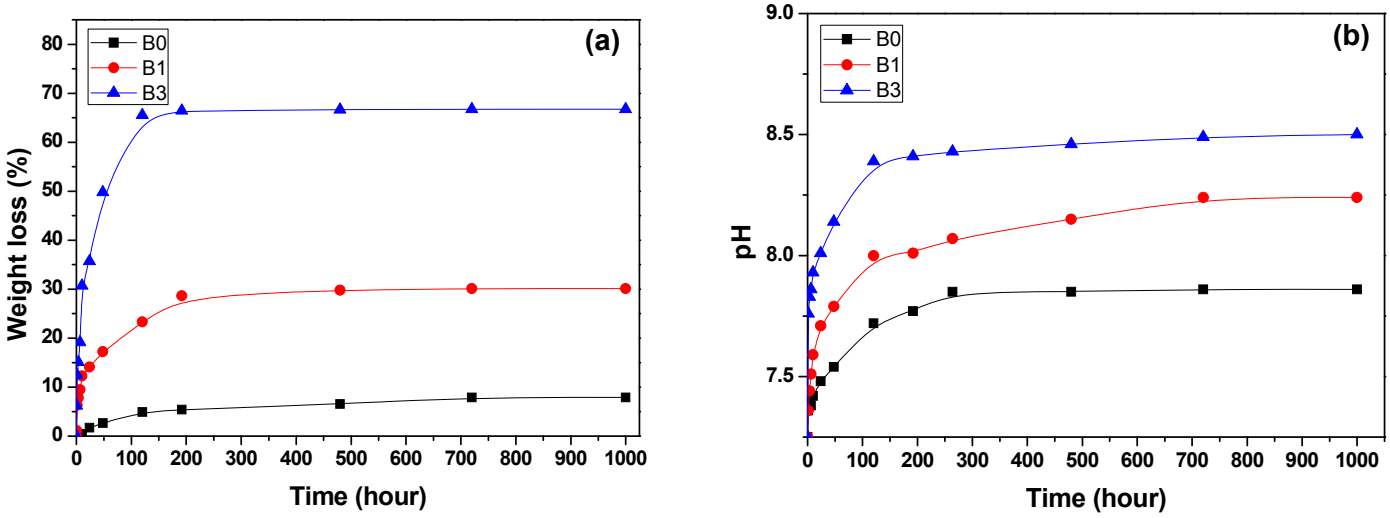

Fig. 4. (a) Weight loss of the scaffold and (b) pH of SBF as a function of immersion time of immersion time of 13-93(B0); 13-93B1, and 13-93B3 scaffolds in a simulated body fluid (SBF). (Rahaman, Missouri S&T).

Figure 5 shows the converted layer on the scaffold surface after 14 days in the SBF. The layer consisted of a porous network of nanometer-sized particles, in which the morphology of the particles changed from needle-like for the 13-93 scaffold to a more spherical shape for the 13-93B3 scaffold. X-ray diffraction (XRD) and Fourier transform infrared (FTIR) analysis confirmed that the converted layer was HA.

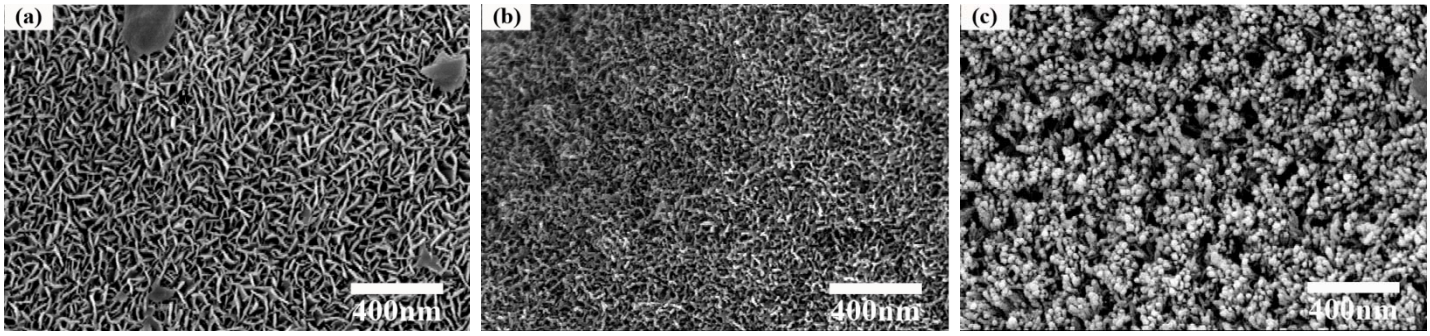

Fig. 5. SEM images of the surface of (a) 13-93 (B0), (b) 13-93B1 and (c) 13-93B3 glass scaffolds after immersion in SBF for 14 days (Rahaman, Missouri S&T).

Mechanical response of scaffolds: Trabecular scaffolds of 13-93, 13-93B1, and 13-93B3 bioactive glass, with a cylindrical shape (6 mm in diameter × 12 mm) were tested in compression (0.5 mm/min) according to ASTM C-773. The scaffolds had a porosity of 75–85% and pores of size 100–500 μm. **Figure 6** shows the stress vs. deformation curves for the 13-93, 13-93B1, and 13-93B3 scaffolds with the trabecular microstructure. The compressive strength, taken as the highest stress on the stress vs. displacement curve, was 11 ± 1 MPa for 13-93, 7.0 ± 0.5 MPa for 13-93B1, and 5.0 ± 0.5 MPa for 13-93B3, showing that the strength decreased with increasing B_2O_3 content of the glass.

When immersed in a SBF, the scaffolds showed a marked decrease in strength as a function of immersion time (**Fig. 7**). The degradation of the strength was dependent on the glass composition. Because of the rapid conversion of the borate 13-93B3 glass to HA, the strength of these scaffolds decreased to almost zero within 4 days. Within the same time, the strength of the as-prepared silicate 13-93 scaffolds decreased to ~30% of its as-prepared strength.

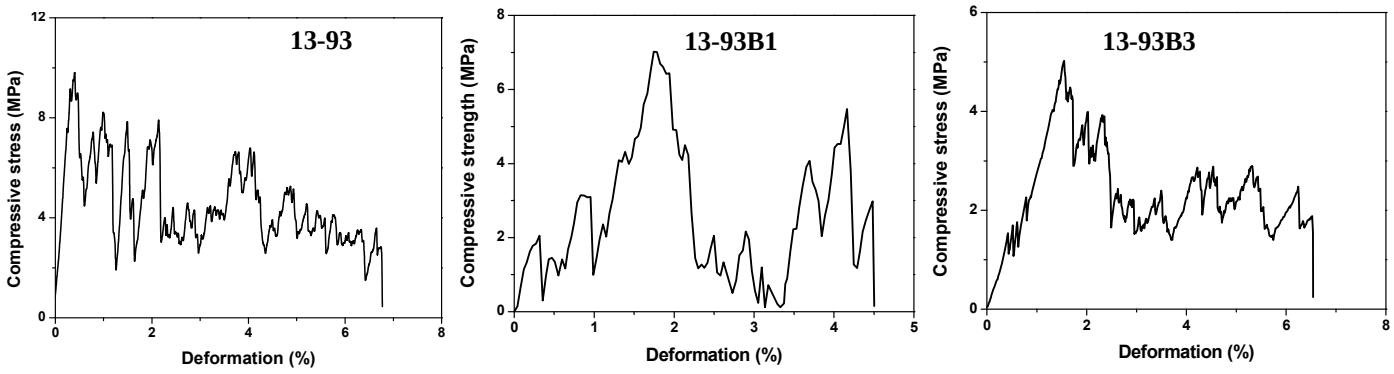

Fig. 6. Stress vs. deformation curves for 13-93, 13-93B1, and 13-93B3 scaffolds with the trabecular microstructure, in compression testing at a deformation rate 0.5 mm/min. (Rahaman, Missouri S&T)

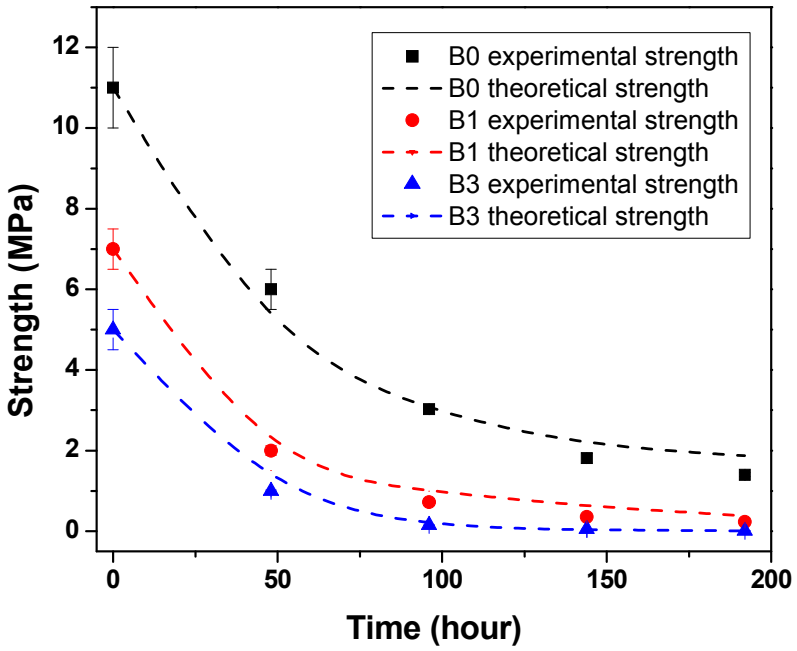

Fig. 7. Compressive strength vs. immersion time in a SBF for silicate 13-93, borosilicate 13-93B1, and borate 13-93B3 scaffolds with the trabecular microstructure (experimental strength). The theoretical strengths were based on a model that compensated for the reduction of the cross-sectional area of the glass struts in the scaffolds resulting from conversion of the glass to a porous HA-type material. (Rahaman, Missouri S&T).

Objective D: Functionalized vs. Non-functionalized Surface (Missouri S&T)

Bonding the bioadhesive peptide Arg-Gly-Asp-Cys (RGDC) to 13-93 glass scaffolds as a means of enhancing the attachment, growth, and function of osteogenic cells was investigated. We are presently determining an appropriate method of covalently attaching RGDC to 13-93, initially using the glass in the form of 1 cm^2 discs to simplify testing. The bonding procedure includes use of the aminosilane coupling agent (3-aminopropyl) trimethoxysilane and the heterobifunctional cross-linker γ-maleimidobutyryloxy-succinimide ester, GMBS (Davis et al., 2002). In a current test, 13-93 discs were treated overnight with 2% aminosilane in 95% EtOH, washed with EtOH, and cured for 1 h at 90 C. The aminosilane-derivatized discs were then placed in GMBS (1 mg/ml pH 7.2 buffer) for 1 h to allow the succinimide group of the GMBS to bond to the free amine of the silane agent. After washing to remove excess GMBS, the treated discs were immersed in 0.5 mg/ml RGDC for 1 h to permit covalent attachment of the Cys of the RGDC to the maleimide end of the GMBS cross-linker. Immediately after washing to remove unbound peptide, these discs plus companion control discs were seeded with 150,000 MLO-A5 cells. The control discs included plain untreated discs plus aminosilane/GMBS discs deactivated by addition of cysteine. Following a 2 h incubation for cell attachment, the cell-seeded samples were washed, fixed in cold 100% EtOH, and stained for 10 min with the DNA-binding fluorochrome Hoechst

33258 (2 μg/ml). The stained samples were examined under an epifluorescence microscope fitted with a DAPI filter to visualize the density and distribution of fluorescently-labeled nuclei.

Representative fluorescent images of three different sample discs (one RGDC disc and two control discs) are included in **Fig. 8**. The RGDC sample had a high density and uniform distribution of fluorescently-labeled nuclei. The untreated discs had a very uneven distribution of nuclei and the density in most of the areas with nuclei was lower. The aminosilane/GMBS disc that was deactivated with cysteine prior to cell seeding also had an uneven distribution and lower density of nuclei. The results of this preliminary test appear to confirm the effectiveness of this method of attaching RGDC to 13-93. We plan to move on to using this method of attaching the peptide to 13-93 fiber scaffolds for testing of enhancement of the attachment, growth, and function of MLO-A5 osteogenic cells.

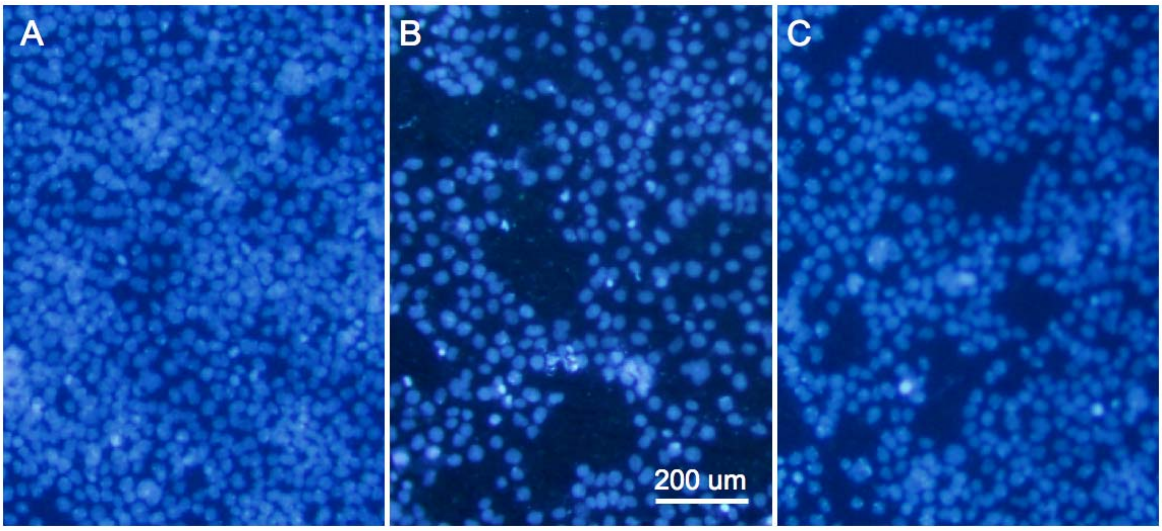

Fig. 8. Fluorescent imaging of relative density and distribution of Hoechst 33258 labeled of cells seeded onto: (A) RGDC coated 13-93 disc; (B) standard untreated13-93 disc; and (C) cysteine deactivated aminosilane/GMBS disc. (Brown, Missouri S&T).

Objective E: In Vitro Cell Culture (Missouri S&T)

The effect of the microstructure and glass composition of the scaffolds on the proliferation and function of MLO-A5 cells, an established osteogenic cell line (Kato et al., 2001), was investigated.

Effect of scaffold microstructure:

Scaffolds of 13-93 glass (~6 mm diameter × ~2.5 mm thick) with the trabecular and fibrous microstructures, prepared as described in Objective C, were dry heat sterilized, preconditioned 1 h in complete medium, blotted dry, and seeded with 50,000 MLO-A5 cells. After cell attachment, the samples were placed in a 24-well plate containing α-MEM medium with 5% fetal bovine serum/5% neonatal calf serum. Incubation was at 37°C in 5% CO_2 with medium changed at 2 day intervals.

SEM visualization: The scanning electron micrographs in **Fig. 9** show the morphology and relative density of MLO-A5 cells on 13-93 fiber and trabecular scaffolds at culture intervals of 2, 4, and 6 days. The cells visible in the images appear well attached on both scaffold types. As a group, the SEM images of **Fig. 9** show a continuing increase in cell density during the 6-day incubation on both the 13-93 fiber and 13-93 trabecular scaffolds, a pattern seen in additional SEM analyses of MLO-A5 cells cultured on these porous constructs.

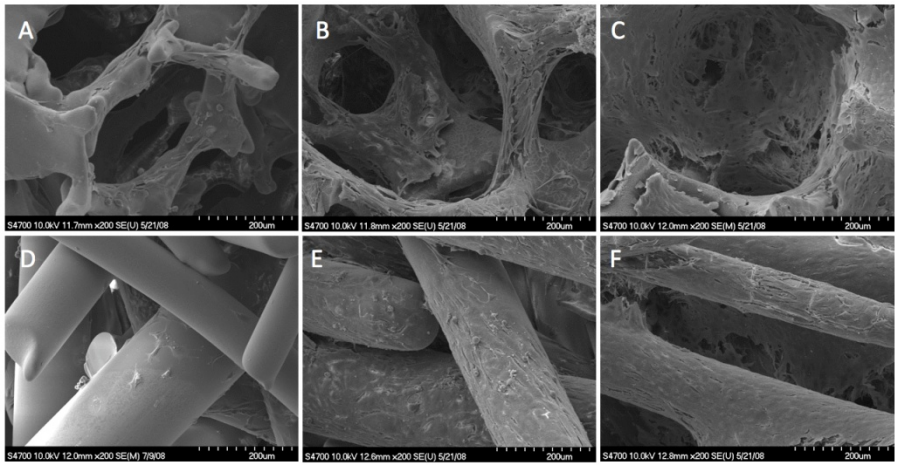

Fig. 9. Scanning electron microscope images of MLO-A5 cells cultured 2 days (A, D), 4 days (B,E), and 6 days (C,F) on fiber scaffolds (A-C) and trabecular scaffolds (D-F). The micrographs show well-attached morphology plus increasing density during the 6 day culture. (Brown, Missouri S&T).

Metabolic activity and growth on scaffolds: The tetrazolium salt MTT was added to cell-seeded scaffolds for the last 4 h of incubations of 2, 4, and 6 days to permit visualization of metabolically active cells on and within the fiber and trabelular scaffolds. The amount of purple formazan, the product of MTT metabolism, visible on the cell-seeded scaffolds increases with incubation duration (**Fig. 10**), an indication of active cell growth on these porous constructs. Particularly noteworthy is the presence of this MTT product within the interior of the scaffolds. The amount of purple formazan visible in the interior, although less than on the surface, suggests there is adequate nutrient permeating the scaffolds to keep cells within the interior in a metabolically active state. The size and interconnectivity of the pores of the fiber and trabecular scaffolds likely accounts for permeation of nutrient and thereby fulfills one of the main properties required for scaffolds designed for use in bone tissue engineering applications.

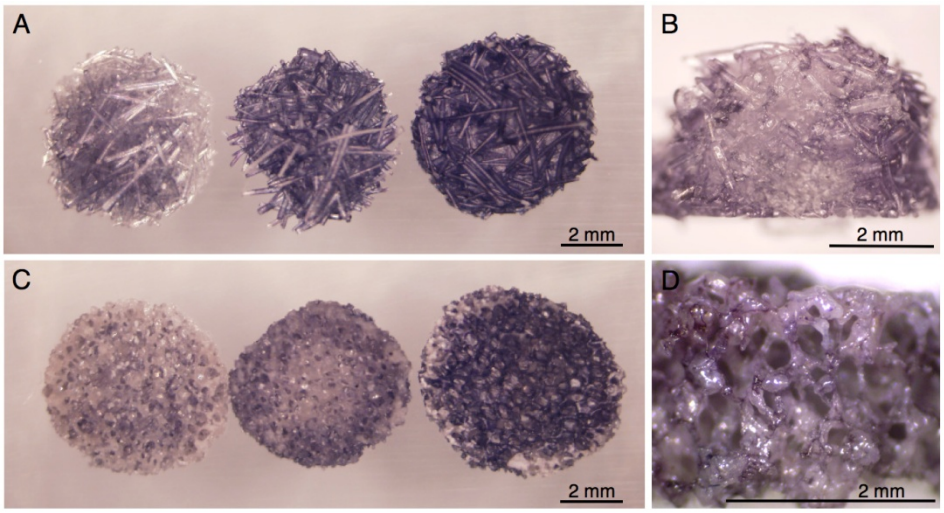

Fig. 10. Bone cell-seeded fiber and trabecular scaffolds treated with MTT for the final 4 h of incubations of 2, 4, and 6 days (panel A and C). The freeze fracture face of cell-seeded fiber and trabecular scaffolds at day 6 are shown in panels B and D, respectively. The latter images show MTT labeled cells within the interior of the scaffolds. (Brown, Missouri S&T).

Total amounts of protein in cellular material recovered from MLO-A5 cells cultured on the fiber and trabecular scaffolds were measured as an additional assessment of ability of the scaffolds to support cell growth. As shown in **Fig. 11**, the amount of protein recovered from the scaffolds increased at a nearly linear rate, a finding that complements the increase in cell density observed in the SEM images.

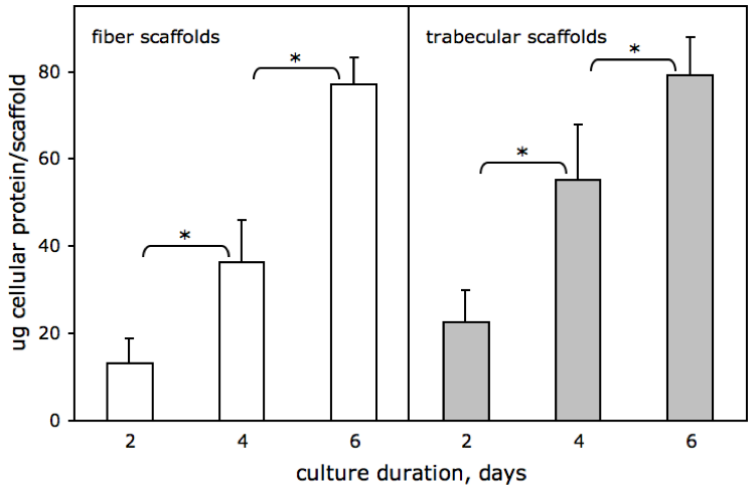

Fig 11. Cell proliferation on 13-93 fiber and trabecular scaffolds assessed by quantitative measurement of total protein. Each bar represents an average of three replicates ± SD. The asterisks indicate statistically significant differences in total protein between culture intervals (p<0.05).

Alkaline phosphatase activity in scaffold cultures: A requirement of scaffolds used for bone tissue engineering applications is the ability to support differentiation of osteoprogenitor cells to functional bone tissue. Alkaline phosphatase (ALP) activity, a well-characterized indicator of the osteogenic phenotype, was measured in MLO-A5 cells cultured on the 13-93 fiber and trabecular scaffolds as a test of differentiated function. Results of spectrophotometric measurements of ALP activity in cell lysates recovered from the scaffolds at culture intervals of 2, 4, and 6 days are presented in **Fig. 12**. As shown, ALP activity increased extensively in these cells with the duration of incubation on the scaffolds. This finding is an indication that the fiber and trabecular scaffolds do effectively support one activity associated with osteogenic function.

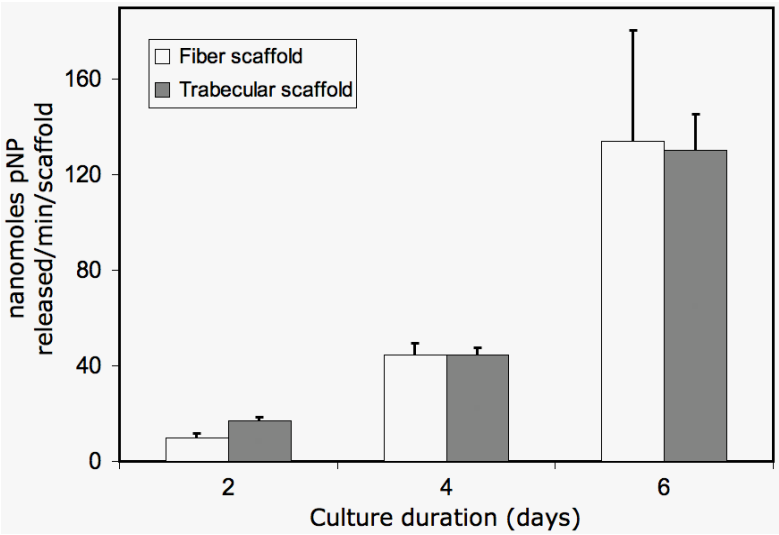

Fig. 12. Alkaline phosphatase activity in MLO-A5 cells cultured on 13-93 glass fiber and trabecular scaffolds. Enzyme activity is expressed as nmol of pNP per minute per scaffold. Average of 3 replicates ± (SD). (Brown, Missouri S&T).

Mineralization on scaffolds: Formation of a mineralized matrix is a defining indicator of the osteogenic phenotype and one of the properties of MLO-A5 cells incubated for an extended duration in mineralization medium (supplemented with ascorbic acid and ß-glycerolphosphate). Measurements of alizarin red staining of mineralized nodules formed by MLO-A5 cells cultured on fiber and trabecular scaffolds are presented in **Fig. 13**. As shown, the addition of mineralization inducing medium caused formation of alizarin red-positive material to increase almost twenty fold compared with that in scaffold cultures maintained in normal control medium. This is further evidence that the 13-93 fiber and trabecular scaffolds support osteogenic differentiation.

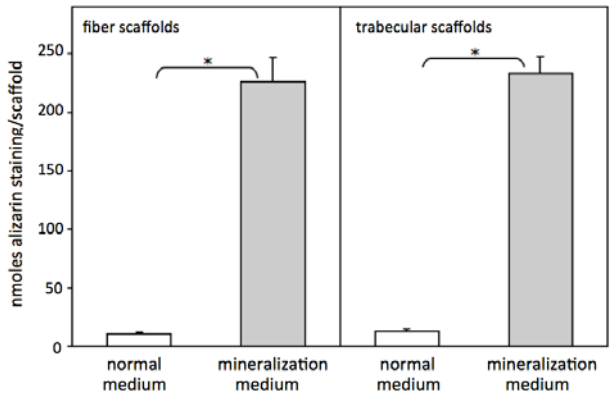

Fig. 13. Comparison of alizarin red staining of mineralized matrix formed by MLO-A5 cells cultured for 12 days on 13-93 fiber and trabecular scaffolds in normal medium vs. mineralization inducing medium. n=3. (Brown, Missouri S&T).

MTT cytotoxicity assay of glass extracts

The 13-93; 19-93B1; and 13-93B3 glasses were pulverized to ≤45 um particles, dry heat sterilized, and then incubated for two days at 50˚C in nanopure water at a concentration of 30 mg/ml. The pH of the resulting aqueous extracts of the 13-93; 19-93B1; and 13-93B3 glasses were found to be 7.8, 9.0, and 9.1, respectively. A portion of each glass extract was adjusted to pH 7.4 and then filter sterilized. Appropriate volumes of the original extract and pH adjusted extract of each glass were added to complete α-MEM medium containing 10% fetal bovine serum. The quantitative cytotoxic assay involving mitochondrial reduction of MTT tetrazolium was used to assess effect of the extracts. MLO-A5 cells were seeded at 5200 cells/well in α-MEM medium with various amounts of the extract in 96-well plates. After 3 days of incubation, MTT was added (50 µg/well) for the last 4 h of incubation. Amounts of purple formazan product formed was measured at 550 nm in a plate reader.

Effects of the addition of original extract and pH adjusted extract of the 13-93, 13-93 B1, and 13-93 B3 glasses are shown in the **Figs. 14 and 15**, respectively. The level of proliferation of MLO-A5 cells cultured in medium containing the original extract and the pH adjusted extract of the standard 13-93 glass was 94 to 105% of control over a wide range of test concentrations (from 0.2 to 10 mg/ml). Addition of increasing amounts of original extract of the 13-93 B1 glass caused a concentration-dependent partial inhibition of MLO-A5 cell growth dropping to approximately 60% of control at glass concentrations of 10 mg/ml. Increasing amounts of neutralized extract of the 13-93 B1 glass caused similar levels of partial inhibition of growth dropping to approximately 65% of control at 10 mg/ml. Incubation of MLO-A5 cell in the presence of the 13-93 B3 glass extracts caused a more dramatic concentration-dependent inhibition of growth. Addition of the original extract and the pH adjusted extract of 13-93 B3 glass at 10 mg/ml decreased cell growth to 18% and 23% of control, respectively.

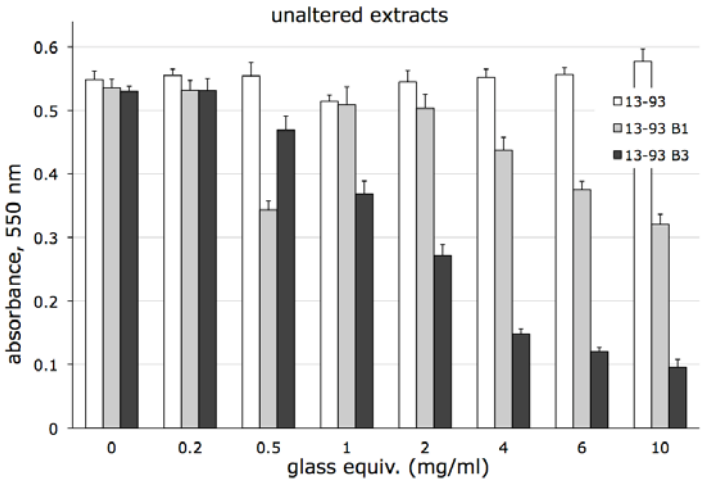

Fig. 14. Evaluation of cytotoxicity of unaltered extracts of 13-93, 13-93B1, and 13-93B3 glasses by MTT hydrolysis. Each bar represents MTT formazan product formed MLO-A5 cells cultured with extract and is an average of five replicates ± SD. (Brown, Missouri S&T).

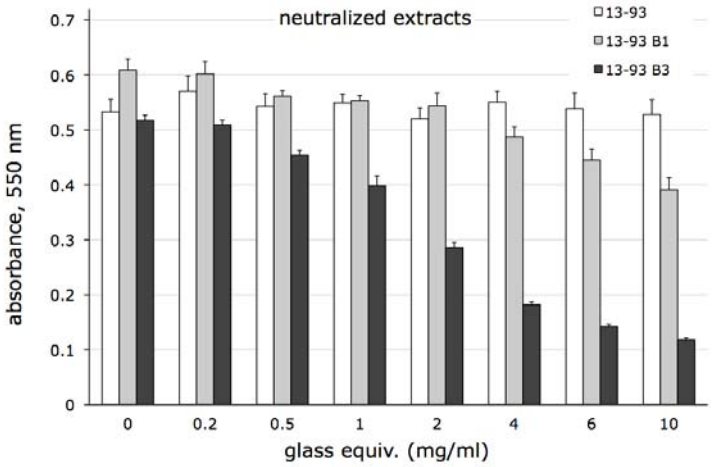

Fig. 15. Evaluation of cytotoxicity of neutralized extracts of 13-93, 13-93B1, and 13-93B3 glasses by MTT hydrolysis. Each bar represents MTT formazan product formed MLO-A5 cells cultured with extract and is an average of five replicates ± SD. (Brown, Missouri S&T).

It was apparent from these tests that the 13-93 B1 glass cause a modest inhibition of cell proliferation, the 13-93 B3 glass causes a more severe inhibition of cell proliferation, and the extract of the standard 13-93 glass has no discernable effect. It was noteworthy that for each of these glass compositions, the levels of inhibition of cell growth by the original unaltered extracts and the neutralized extracts were nearly the same. These and other related results suggest that the modest to severe inhibition of cell growth by 13-93 B1 and 13-93 B3 glasses occurs by a mode of action other that a pH effect.

Assessment of biocompatibility

An additional procedure used to compare the relative levels of biocompatibility of the 13-93, 13-93 B1, and 13-93 B3 glasses was a qualitative assay of cell morphology and density. MLO-A5 cells were seeded in 12-well plates in α-MEM medium with 6 mg/ml of the various extracts. After incubations of 1 day and 3 days, the cell morphologies and relative densities of the cells were compared to qualitatively assess the biocompatibility of the glass extracts.

Representative images of the morphology and relative densities of MLO-A5 cells after 1 day and 3 days of culture in the presence of 13-93, 13-93 B1, and 13-93 B3 extracts are shown in **Fig. 16**. Cells incubated with 13-93 extract are well attached to the plate, show the spread, attached morphology characteristic of the MLO-A5 cell line, and underwent dramatically increased cell density between day 1 and day 3. Cells incubated with the 13-93 B1 extract have a lesser increase in cell density and do not show the typical morphology. Incubation with the 13-93 B3 extract resulted in rounded, poorly-attached cells with very little increase in cell density between day 1 and day 3. Overall these results reveal the 13-93 B1 glass has reduced biocompatibility compared to the standard 13-93 glass while the 13-93 B3 compositions is clearly cytotoxic.

Static vs. dynamic culture of MLO-A5 cells

As part of this phase of the project, tests were performed to compare cell growth on the scaffolds during incubation under two conditions. One was standard incubation with cell-seeded scaffolds in non-mobile 60 mm dishes ('static') in the CO_2 incubator. The second condition was with scaffolds in dishes on a platform rocker set at 30 oscillations/min and positioned in the CO_2 incubator ('dynamic'). Following a 4-day incubation under the static and dynamic conditions, MLO-A5 seeded scaffolds were labeled with MTT. The static incubation resulted in labeling mostly on the scaffold surface with much less labeling in the interior. In contrast, the dynamic incubation yielded more homogeneous labeling with dark purple formazan product visible nearly uniformly throughout the scaffold suggesting that the dynamic incubation allowed greater delivery of nutrient to cells in the exterior thereby allowing a more uniform growth.

In a similar manner, dynamic incubation was tested as a way of enhancing growth of MLO-A5 cells on 13-93 B3 glass scaffolds, the glass with very low biocompatiblility. The photograph image in **Fig. 17** compares the pattern of MTT labeling of MLO-A5 seeded 13-93 B3 scaffolds after 2 day culture under static and dynamic conditions. The static incubation resulted in very little labeled with MTT. In contrast, the dynamic incubation

yielded much greater labeling with MTT indicating the presence of more cells on the scaffolds. This indicates the dynamic incubation allowed reduction of the toxicity of the 13-93 B3 glass.

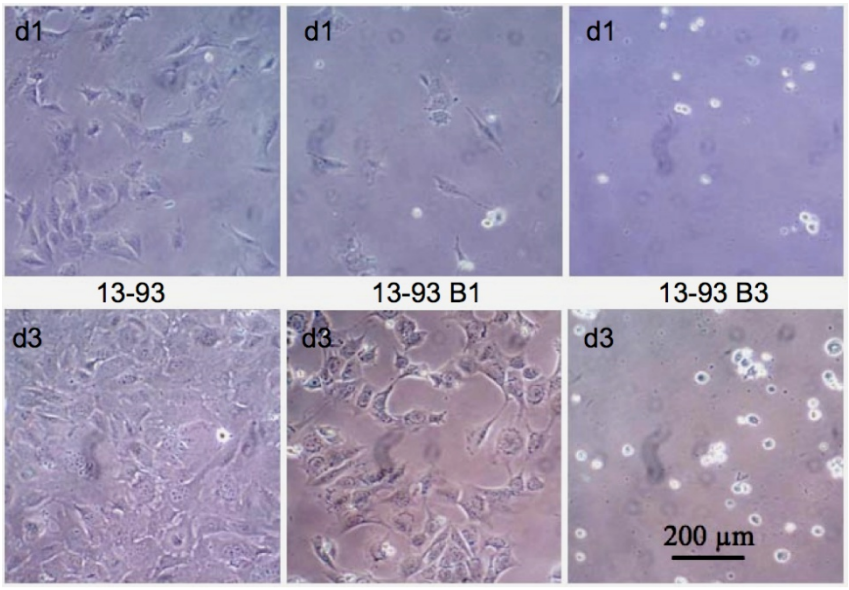

Fig. 16. Phase contrast images of MLO-A5 cells in medium with neutralized extracts of 13-93, 13-93B1, and 13-93B3 glass (6 mg/ml) at d1 and d3 of culture. (Brown, Missouri S&T).

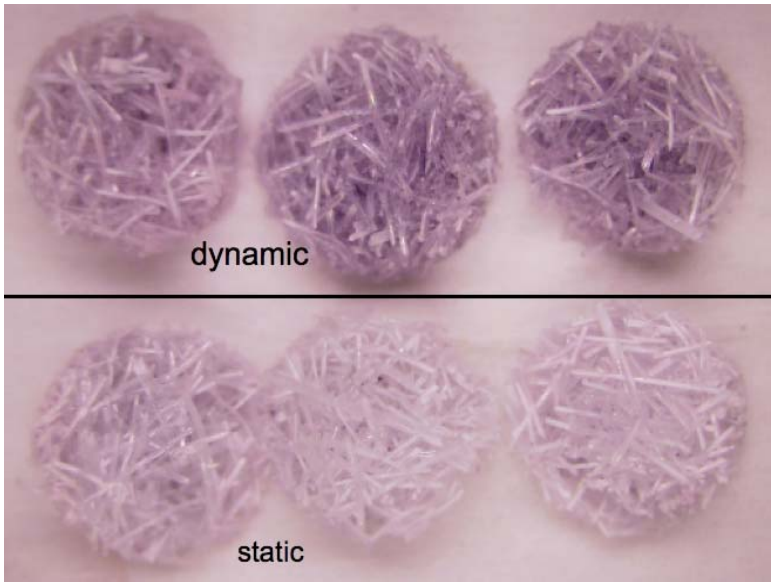

Fig 17. MTT labeling of cell-seeded 13-93 B3 scaffolds incubated 2 days under dynamic and static conditions. (Brown, Missouri S&T).

Effect of scaffold glass composition:

The composition of the glass scaffold also had a marked effect on its ability to support proliferation and function of MLO-A5 cells.

Scaffolds of 13-93, 13-93B1 and 13-93B3 bioactive glass (6mm in diameter × 2 mm thick) with the trabecular microstructure were sterilized by washing 3 times with water and ethanol (for 13-93 and 13-93B1 compositions) or ethanol (for 13-93B3 composition), followed by heating for 24 h at 500ºC. The scaffolds were each seeded with 50,000 MLO-A5 cells suspended in 40 µl medium. After incubating for 4 h to permit cell

attachment, the cell-seeded scaffolds were transferred to a 24-well culture plate containing 2 ml of complete medium per well. At selected time intervals, the glass scaffolds with attached cells were removed for assays.

Cell viability: The effect of glass composition on the viability of MLO-A5 cells was assessed using a live cell/dead cell assay. After culturing for different intervals, the trabecular scaffolds with attached cells were rinsed gently with warm phosphate-buffered saline (PBS), and incubated for additional 30 min in 2 ml serum-free medium containing 2 μM calcein AM and 2 μM ethidium homodimer, EthD-1 (Invitrogen Corp, Carlsbad, CA). The fluorochrome labeling of the MLO-A5 cells showed a marked increase in cell number with culture time for the 13-93 and 13-93B1 scaffolds, with very few dead cells (**Fig. 18**). On the other hand, no increase in cell number was observed for the 13-93B3 scaffolds, and a few dead cells were found on these scaffolds at all culture times. These cell viability results for the porous scaffolds are consistent with the results in Fig. 1a for cell proliferation of MLO-A5 cells on dense discs of 13-93, 13-93B1, and 13-93B3 glass.

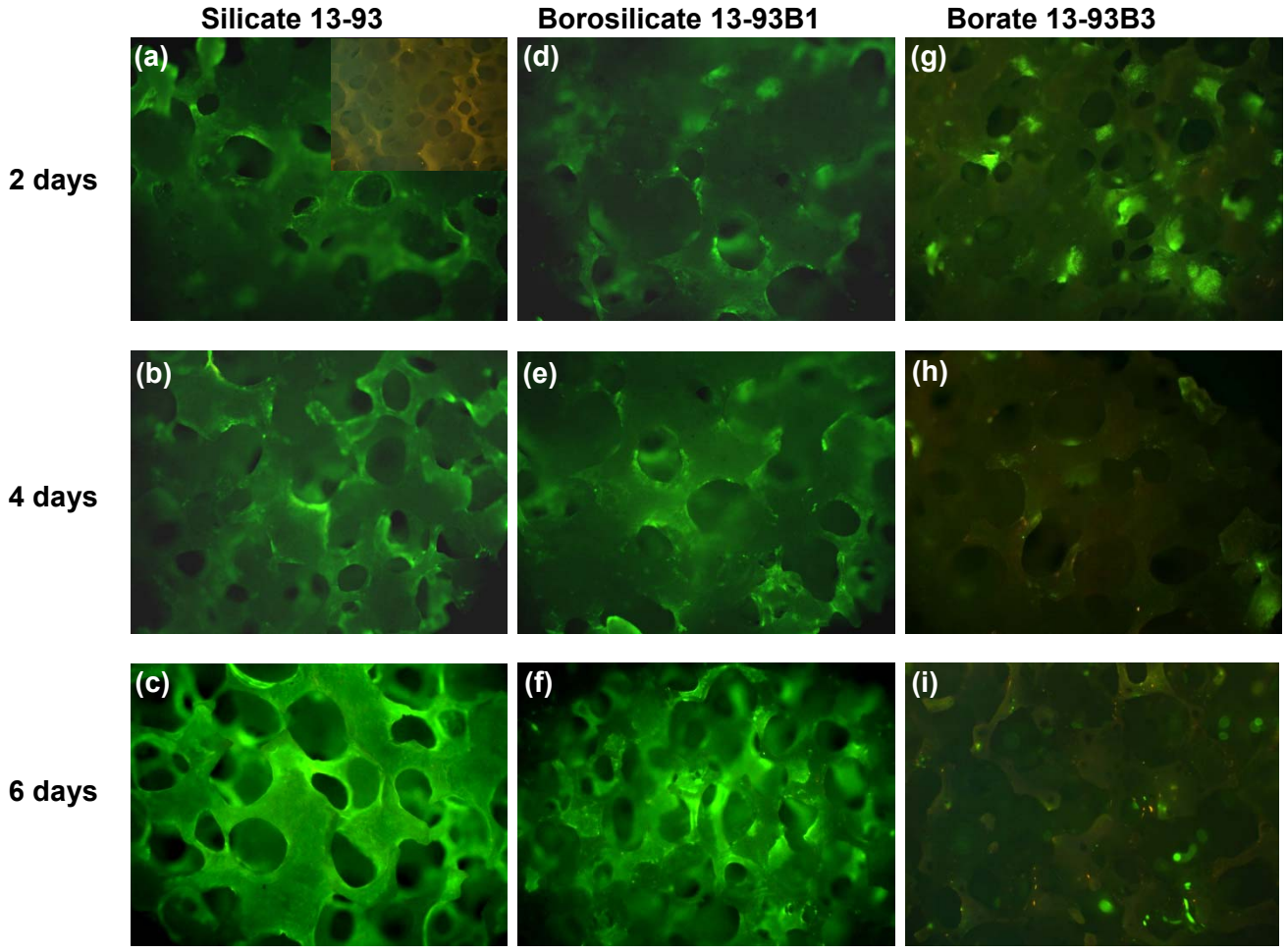

Fig. 18. Fluorescent images of MLO-A5 cells cultured on 13-93, 13-93B1, and 13-93B3 scaffolds (left to right) for 2, 4, and 6 days (top to bottom). The inset in (a) shows an image of a 13-93 scaffold without cells. (Rahaman et al., Missouri S&T).

Cell proliferation: Total amount of protein in lysates recovered from the cell-seeded trabecular scaffolds were measured with a micro-BCA Protein Assay Kit (Piece Biotechnology, Rockford, IL). The scaffolds were placed in 500 μl of 1% Triton X-100 and the cells were lysed by two freeze-thaw cycles (-80/37 ºC). Sample absorbance values were measured at 550 nm in a BMG FLUORstar Optima plate reader with bovine serum albumin used as a standard for comparison. The amount of protein (**Fig. 19**) showed a nearly linear increase in cell proliferation during the 6 day incubation for the 13-93 and 13-93B1 bioactive glass scaffolds, a finding that complemented the progressive increase in cell density in the live cell/dead cell assays. On the other hand, no significant increase in the amount of protein was found on the 13-93B3 scaffolds, an indication of the inhibiting effects of this scaffold on cell proliferation.

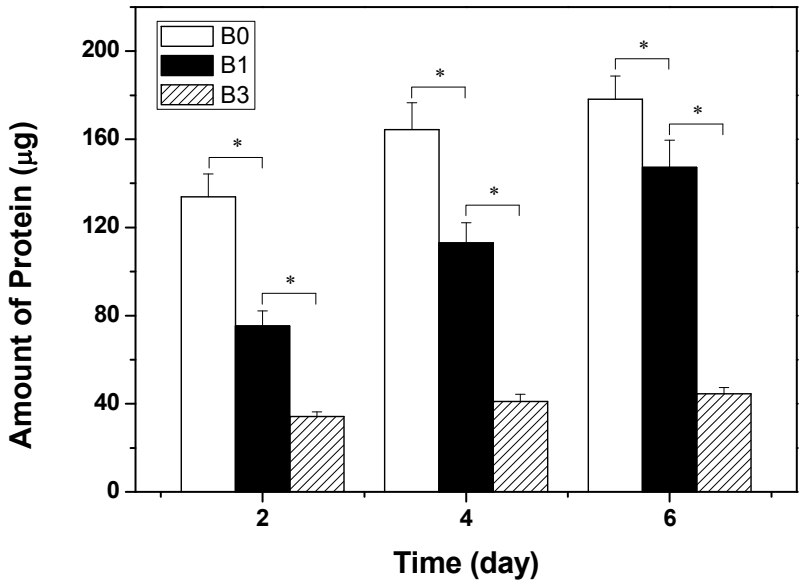

Fig. 19. Ability of 13-93(B0), 13-93B1, and 13-93B3 bioactive glass scaffolds with ability of trabecular microstructure to support proliferation of MLO-A5 cells. Mean ± sd; n = 4. *Significant difference for glass scaffolds with different compositions (p<0.01). (Rahaman, Missouri S&T.)

Alkaline phosphatase activity: The cell-seeded scaffolds were removed at selected time intervals and the cells were lysed using two -80/37ºC cycles. The spectrophotometric measurement of alkaline phosphatase (ALP) in the lysate was conducted with p-nitrophenyl phosphate (p-NPP) substrate as described elsewhere (Sabokar et al., 1994). The ALP activity increased with incubation time for the 13-93 and 13-93B1 scaffolds (**Fig. 20**), an indication that the cells were able to carry out an osteogenic function on these two groups of scaffolds. The much lower and almost stable ALP activity for the 13-93B3 scaffolds during the incubation time was an indication of the poor biocompatibility of the scaffolds.

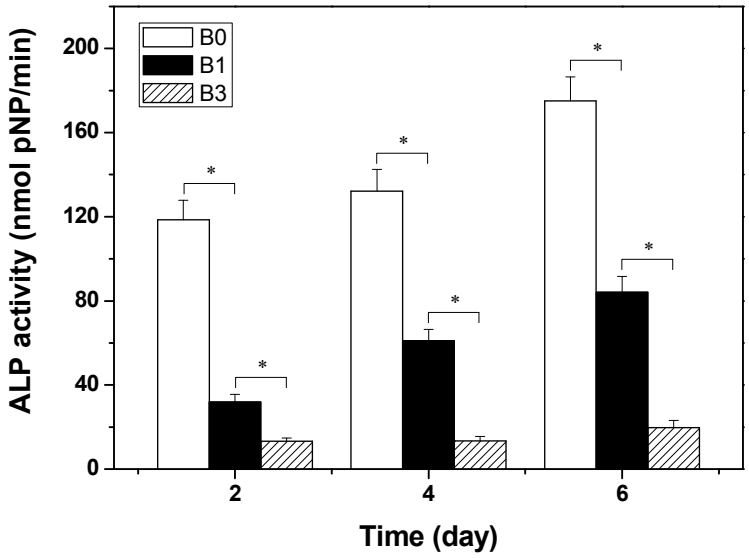

Fig. 20. Ability of 13-93(B0), 13-93B1, and 13-93B3 bioactive glass scaffolds with the trabecular microstructure to support differentiated function of MLO-A5 cells. Mean ± sd; n = 4. *Significant difference for glass scaffolds with different compositions (p<0.01). (Rahaman, Missouri S&T.)

Objective F: *In Vivo* Studies (Missouri S&T)

Implantation of selected groups of bioactive glass scaffolds in a bone defect model (rat calvaria defects) is a focus of the Year 2 tasks. In preparation for the Year 2 experiments, we evaluated the *in vivo* biocompatibility of the fibrous and trabecular scaffolds in a subcutaneous rat implantation model.

Fibrous scaffolds: Scaffolds of 13-93 and 13-93B3 bioactive glass (7mm in diameter and 2mm thick), half seeded with 50,000 mesenchymal stem cells (MSCs), half in the as-made condition (unseeded), were placed in subcutaneous pockets in the back of a Fisher 344 rat. After six weeks *in vivo*, the scaffolds were removed and processed for histology and SEM analysis.

Assessment of 13-93B3 fibrous scaffolds after implantation for 4 weeks: An as-made scaffold of 13-93B3 was encased in plastic and sectioned as a standard on how the fibers looked prior to implantation. The image (**Fig. 21**) shows several fibers bonded together, and the fibers themselves look rounded. Since the scaffold is comprised of a random fiber orientation, some of the fibers will look elongated as they were cut off center. An H&E stained section of the 13-93B3 scaffold implanted for 4 weeks is shown in **Fig. 22**. The fibers are completely surrounded by soft tissue, and the fibers are no longer solid as in the as-made example above. The fibers have become hollow, and in many cases are filled with tissue.

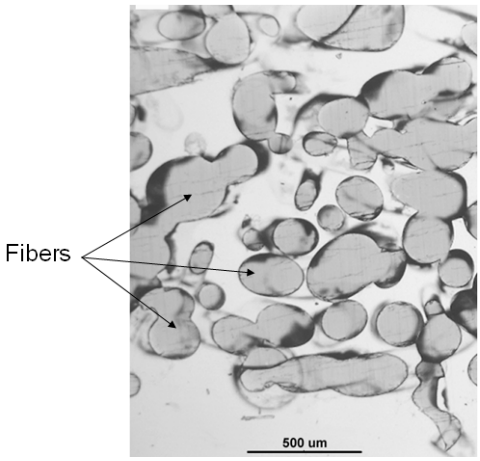

Fig. 21. Optical image of the cross section of an as-prepared 13-93B3 fibrous scaffold. (Day, Missouri S&T)

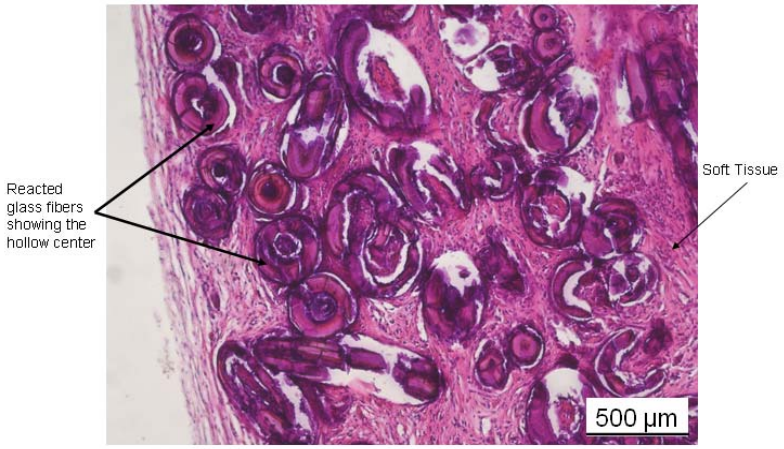

Fig. 22. Transmitted light image of an H&E stained section of 13-93B3 bioactive glass scaffold after implantation for 4 weeks. (Day, Missouri S&T)

Further analysis of the scaffold was done using SEM, as a scaffold was sectioned and imaged. The fibers again are hollow and in many cases filled with soft tissue. The center of a hollow fiber was magnified, and at highest magnification, nano crystals of a material that looked similar to hydroxyapatite (HA) were present (**Fig. 23**).

X-ray diffraction was used to verify that the nano crystals seen in the SEM analysis were in fact HA. **Figure 24** shows the XRD pattern for a 13-93B3 scaffold implanted for 4 weeks as described above, and the crystalline material was identified as HA from the PDF database (card number 72-1243).

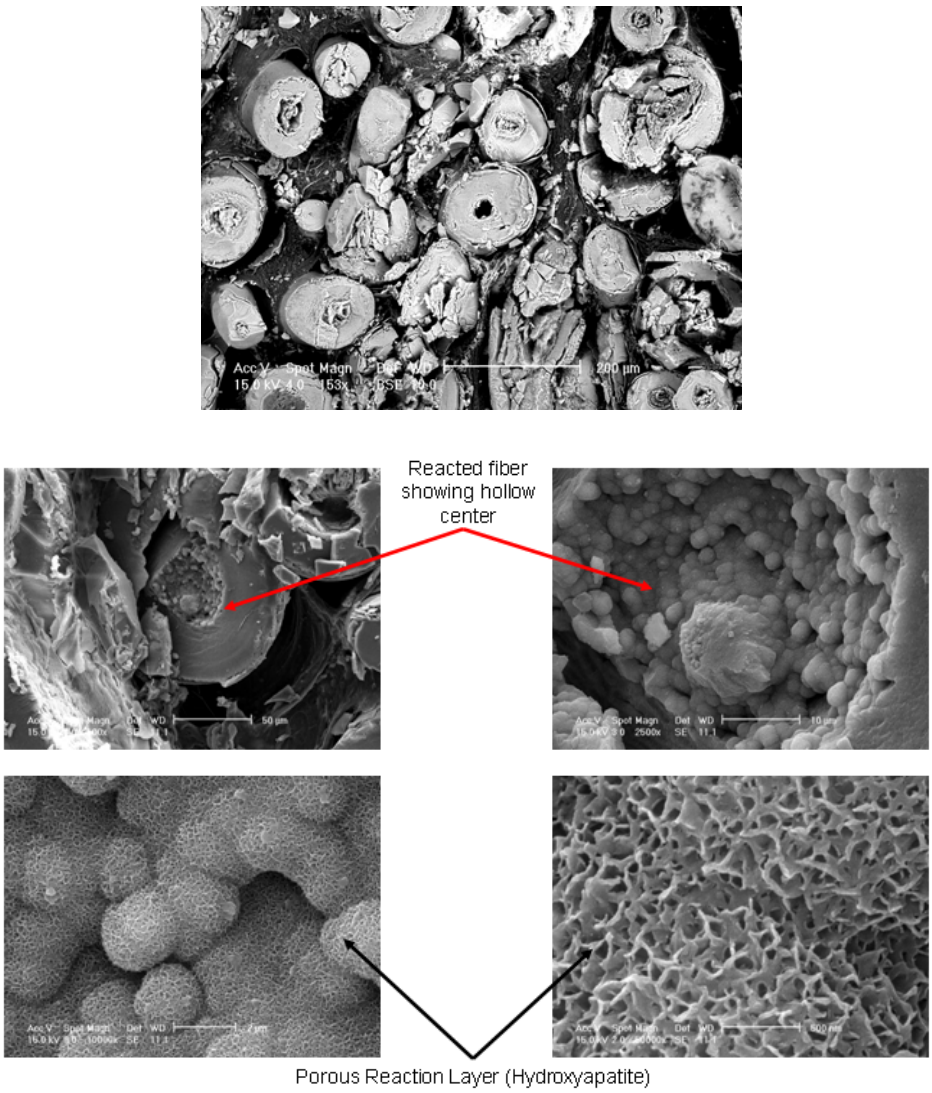

Fig. 23. SEM images of 13-93B3 scaffolds with the fibrous microstructure after subcutaneous implantation for 4 weeks. (Day, Missouri S&T)

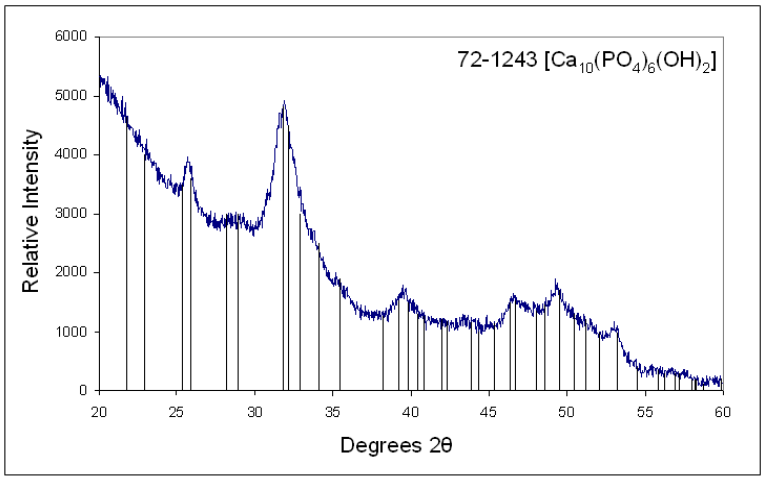

Fig. 24. XRD pattern of 13-93B3 bioactive glass scaffold after implantation for 4 weeks. The pattern of a reference hydroxyapatite (JCPDS 72-1243) is shown for comparison. (Day, Missouri S&T).

Assessment of 13-93 fibrous scaffolds after implantation for 4 weeks: Scaffolds (7 mm in diameter × 2 mm), one group seeded with 50,000 mesenchymal stem cells (MSCs), and another group in the as-made condition (unseeded), were placed in subcutaneous pockets in the back of Fisher 344 rats and incubated for 3 and 4 weeks. Upon extraction, all the scaffolds were completely filled with soft tissue with several areas containing visible blood vessels penetrating the scaffolds (**Fig. 25**).

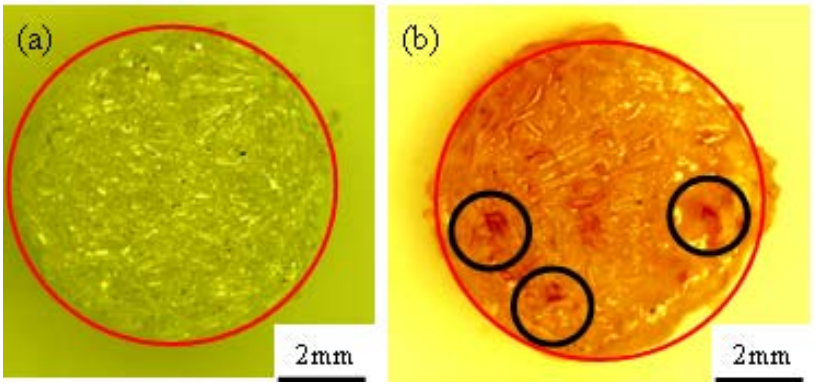

Fig. 25. Optical micrographs of 13-93 bioactive glass scaffolds with the fibrous microstructure (a) as-made scaffold; (b) after seeding with MSCs and implanted for 4 weeks in subcutaneous pockets in the dorsum of Fisher 344 rats. The red circle is 7 mm in diameter and denotes the starting diameter of each scaffold (Day, Brown; Missouri S&T).

Subsequent sectioning and staining of the scaffolds identified both soft and hard (bone) tissue in the MSC-seeded scaffolds, whereas the as-made scaffolds only contained soft tissue (**Fig. 26**).

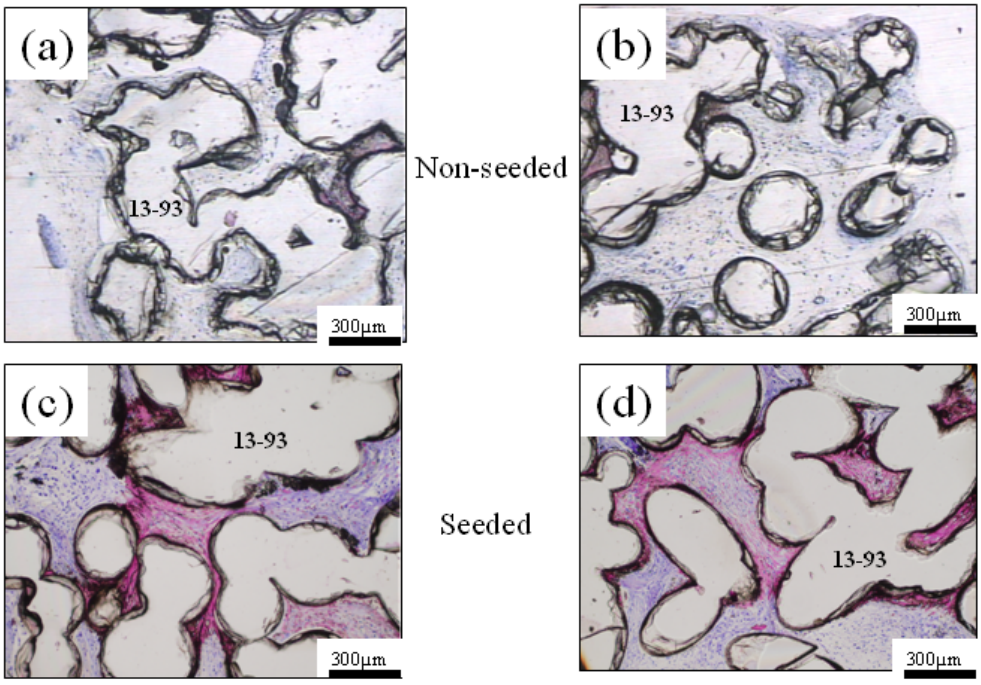

Fig. 26. Optical micrographs of the cross section of 13-93 bioactive glass scaffolds with the fibrous microstructure after subcutaneous implantation for 3 weeks (a), (c), or 4 weeks (b), (d). Blue tissue represents soft tissue, whereas red represents hard (bone) tissue. (Day, Brown; Missouri S&T)

Back-scattered electron (BSE) images taken in the SEM (**Fig. 27**), coupled with energy-dispersive X-ray (EDS) analysis of sections of the MSC-seeded scaffolds, confirmed that the areas stained positive for bone was a calcium phosphate material, with a composition similar to that of stoichiometric hydroxyapatite (HA).

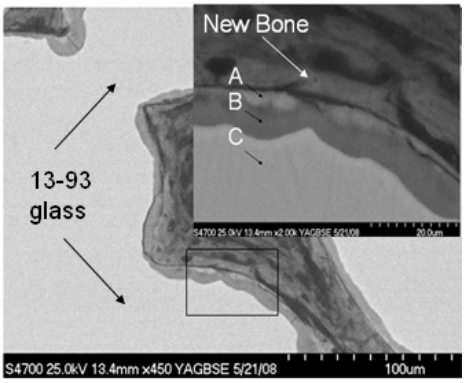

Fig. 27. SEM back-scattered electron image of a section of a MSC-seeded scaffold after implantation for 4 weeks. The magnified view (inset) shows new bone growing adjacent to 13-93 glass fiber. The area labeled A is a calcium phosphate-rich region similar in composition to HA, area B is a silica-rich region, and area C is the unreacted 13-93 glass. (Day, Missouri S&T).

Trabecular scaffolds:

Figure 28 shows the gross appearance of a MSC-seeded trabecular scaffold (13-93) after subcutaneous implantation for 4 weeks. After 4 weeks *in vivo*, a calcium phosphate layer, with a Ca/P ratio corresponding to that of hydroxyapatite (HA), ~20 μm thick, was formed on the surface of the 13-93 bioactive glass of the trabecular scaffold (**Fig. 29a, 29b**).

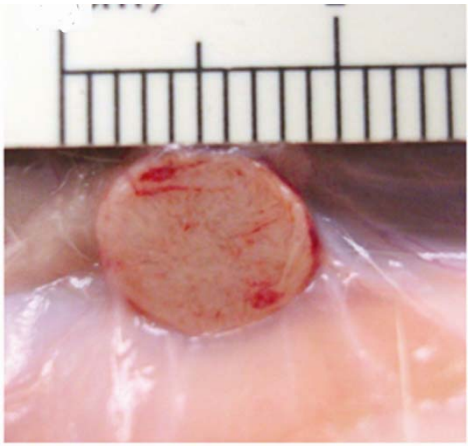

Fig. 28. Gross appearance of 13-93 bioactive glass scaffold after implantation for 4 weeks in subcutaneous pockets in the dorsum of Fisher 344 rats. (The scale is in mm.) (Rahaman, Missouri S&T).

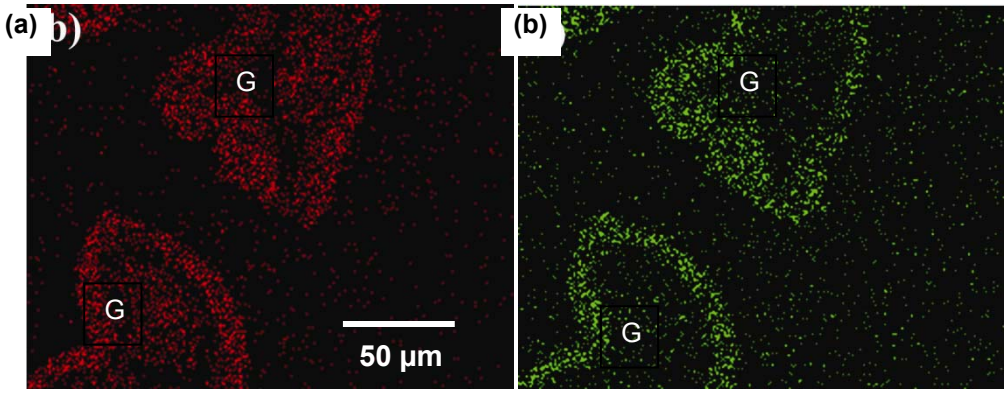

Fig. 29. X-ray maps for (a) Ca(K) and (b) P(K), respectively, of a 'trabecular' scaffold (G), showing a hydroxyapatite-type layer (~20 μm thick) formed on the glass surface (Rahaman, Missouri S&T).

Sections of trabecular scaffolds (13-93, 13-93B1, and 13-93B3), 6 weeks post implantation, were stained with hematoxylin and eosin (H&E), toluidine blue, and Goldner's trichrome. Transmitted light images (**Fig. 30**) showed abundant tissue infiltration into the scaffolds. The intra-glass stroma in 13-93B3 appeared to be less fibrillar when compared to 13-93 and 13-93B1, while the stroma in 13-93B1 appear to be more abundant than in 13-93. Further evaluation of these implants is in progress.

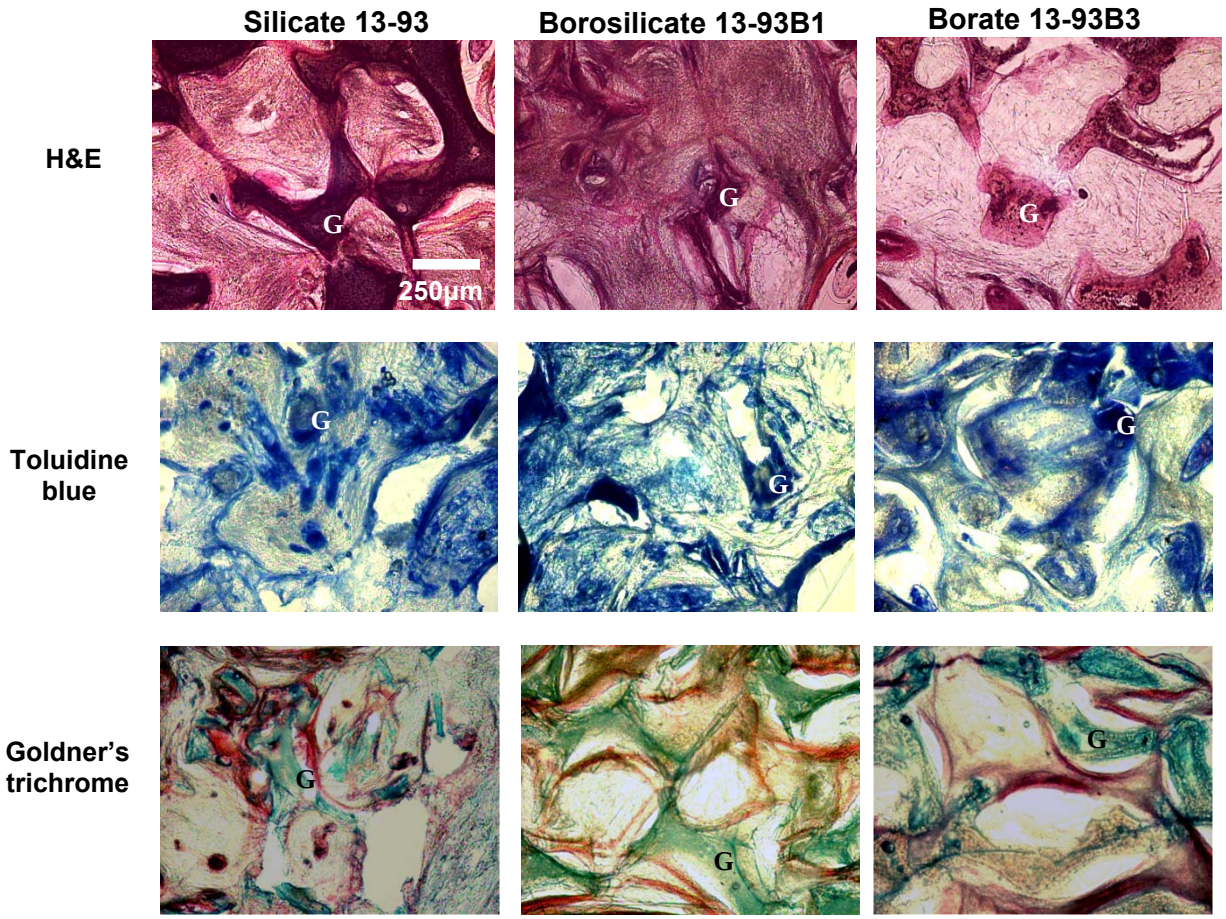

Fig. 30. Transmitted light images of H&E, toluidine blue, and Goldner's trichrome stained sections of trabecular scaffolds with the 13-93, 13-93B1, and 13-93B3 composition after subcutaneous implantation for 6 weeks in the dorsum of Fisher 344 rats. (All images have the same magnification as that for H&E stained 13-93; G denotes the scaffold.) (Rahaman, Missouri S&T).

In vivo skinfold experiment

As part of this phase of the project, we also attempted to use a dorsal skinfold window chamber procedure (Rucker et al., 2006) to monitor a possible angiogenic response to 3mm diameter 13-93 and 13-93B3 glass scaffolds. Three separate trial surgeries were performed which involved implanting a single skinfold chamber in the dorsum of each of six adult Sprague-Dawley rats (four animals with scaffolds and two used as sham controls). Our objective was to photographically record at 3-4 day intervals the macroscopically responses to the scaffolds. The images in **Fig. 31** show tissue around a 13-93 scaffold and a 13-93B3 glass scaffold at 14 days after implantation. Due to the limited number of samples implanted we have been unable to see a clear pattern in differences in vascular density surrounding the two types of scaffolds as well as difference from that seen in the sham controls. Because these surgeries are very time-consuming and permit inclusion of a very limited number of samples, we are presently exploring other possible approaches for visualization of angiogenic responses to the test scaffolds.

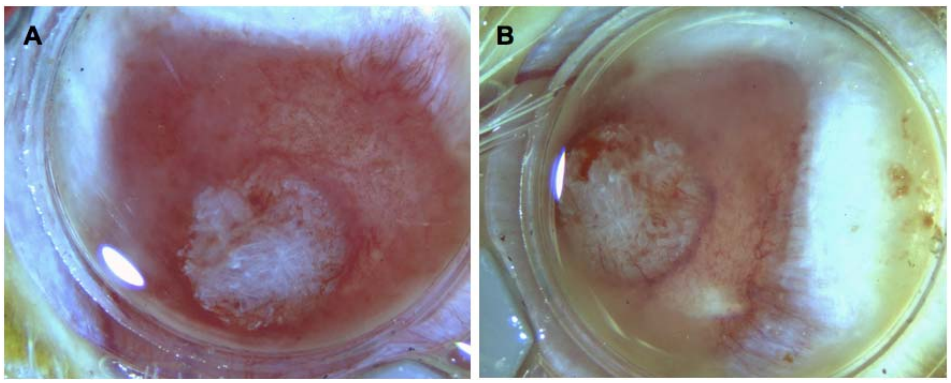

Fig. 31. Macrophotographic images of tissue around a 13-93 scaffold (A) and a 13-93B3 glass scaffold (B) at 14 days after implantation. Window diameter of the skinfold chamber is 10 mm. (Brown, Missouri S&T).

Micro-computed tomography (microCT) evaluation of implanted scaffolds (UMKC)

For the upcoming implantation into rat calvaria defects to be performed in Year 2, scaffolds composed of 13-93 glass were prepared at Missouri S&T and scanned using microCT at UMKC to determine whether soft or hard (bone) tissue in the scaffold was detectable by CT. Examples of the scans are shown in **Fig. 32**, imaged on the day of placement. The scan in **Fig. 32a** is a top view, and the scan in **Fig. 32b** is a reconstructed vertical section from the center of the scaffold. Both images show two preparations of the 13-93 bioactive glass, the left view in each image is random glass preparation (fibrous microstructure) and the right view is an oriented microstructure of unidirectional fibers.

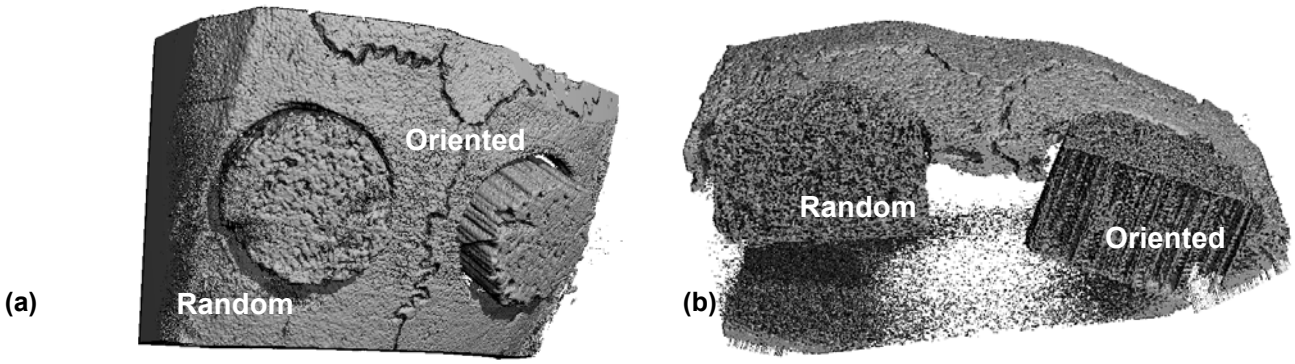

Fig. 32. MicroCT scans of 13-93 bioactive glass scaffolds imaged on the day of placement into rat calvaria defects. (a) top view; (b) reconstructed vertical section from the center of the scaffold. (Bonewald, UMKC).

Biosensors Research and Education (Missouri S&T)

As part of the research and education activities of the Consortium, continuous monitoring of the degradation of bioactive glasses in an aqueous solution was investigated. The following work has been completed towards the determination of chemical concentration in the vicinity of degrading bioactive glass materials using off-the-shelf optical microscopes.

Continuous monitoring of bioactive glass degradation and resulting chemical microenvironment through fluorescent sensing strips

Fluorescence microscopy for chemical environment monitoring: A microscope image is collected using a standard CCD or CMOS camera and stored as an reg/green/blue (RGB) image. The collected image is then processed so that the red, green, and blue pixels are separated. Fluorescence excitation is limited to the blue channel and this value is discarded. Fluorophore emission is limited to the green and red channels, and information of the chemical microenvironment is obtained from these values. A test environment was

constructed as shown in **Fig. 33**. The impermeable substrate layer creates a no-flux boundary condition, mimicking a plane of symmetry for the test cell. The experimental conditions therefore approximate the conversion of a bioactive glass sample of twice the thickness embedded completely within a tissue phantom.

Fig. 33. Bioglass conversion test environment. Fluorescent sensing strips/films that are sensitive to oxygen concentrations or pH are mounted on substrate. Illumination by blue light from above leads to fluorescence and collection of the image through a standard CMOS or CCD camera. (Henthorn and Kim, Missouri S&T).

Ruthenium-containing fluorophore sensing strips for oxygen concentration monitoring: Initial experiments with this test environment were conducted to study whether bioactive glass degradation conditions (significant increase in pH, appreciable consumption of dissolved phosphate) interfered with the sensing capabilities of our oxygen-sensitive materials. **Figure 34** shows a processed image where only the red channel is retained for a bioactive glass sample in a controlled oxygen environment. Experiments with altered pH or phosphate concentrations were conducted in order to establish the robustness of this fluorophore film, and no oxygen signal degradation was noted over the pH levels or phosphate concentration range of interest.

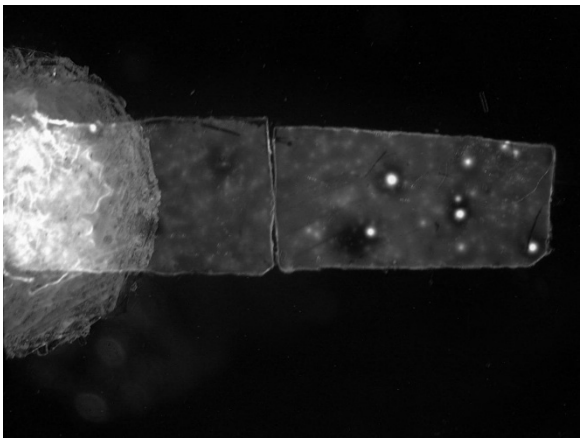

Fig. 34. Red channel image of oxygen-sensitive fluorescent sensor strip in contact with cylindrical bioglass sample (diameter of bioglass sample approximately 2 mm) in a controlled oxygen environment.

pH-sensitive membrane fabrication and evaluation: Fluorophore (ETH5350) was mixed in poly(vinyl chloride) polymer at 1.5% w/w following plasticization with dioctyl sebacate (65% w/w). Proton conduction in the hydrophobic membrane was enhanced through addition of a liphophilic salt, potassium tetrakis(4-chlorophenyl)borate, at 1% w/w. One hundred milligrams of this polymer mixture was dissolved in 0.75 ml THF. This mixture was then spun coated on glass substrate to form a 70 micron thick film. Excitation with blue LED sources (480 nm peak wavelength) resulted in emissions in the green and red. **Figure 35** shows the ratio of the fluorescent emission intensity in the green (565nm) versus that in the red (673 nm) and the effectiveness of the pH sensing properties of this material. Samples were tested on a range of pH adjusted phosphate buffer solutions from 7.2 to 8.9.

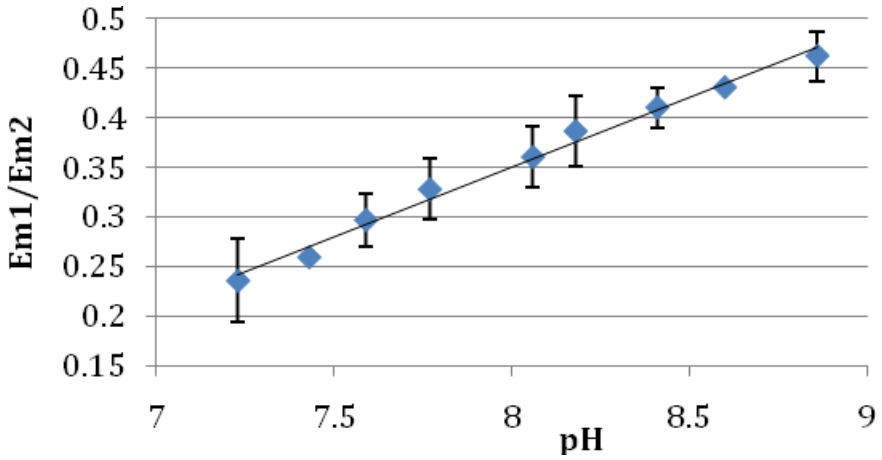

Fig. 35. Ratiometric pH determination using green and red emissions (Em1 = 565nm, Em2 = 673nm) from spun coated fluorophore-containing film

KEY RESEARCH ACCOMPLISHMENTS

- Prepared three candidate bioactive glasses with silicate (13-93), borosilicate (13-93B1), and borate (13-93B3) composition, as well as the widely studied silicate 45S5 glass (control);
- Converted three glasses (13-93; 13-93B1; 13-93B3) into porous three-dimensional scaffolds with two different microstructures (described as 'fibrous' and 'trabecular');
- Evaluated the *in vitro* bioactivity (conversion to a hydroxyapatite-type material in a simulated body fluid) and mechanical response of 13-93, 13-93B1, and 13-93B3 bioactive glass scaffolds with fibrous and trabecular microstructures;
- Evaluated *in vitro* response of MLO-A5 cells (an established osteogenic cell line) to scaffolds of 13-93 bioactive glass with fibrous and trabecular microstructures;
- Evaluated *in vitro* response of MLO-A5 cells to bioactive glasses and glass scaffolds of three different compositions (13-93, 13-93B1, and 13-93B3);
- Evaluated the ability of 13-93, 13-93B1, and 13-93B3 bioactive glass scaffolds with the fibrous and trabecular microstructures to support tissue infiltration in a subcutaneous rat implantation model;
- Initiated *in vivo* experiments: implantation of 13-93 and 13-93B3 scaffolds in dorsal skinfold chambers in rats to assess possible angiogenic responses;
- Initiated *in vitro* tests of covalently bonding a bioadhesive peptide to 13-93 glass scaffolds as a means of enhancing the attachment, growth, and function of osteogenic cells;
- Prepared scaffolds for implantation into rat calvaria defect model in Year 2, and imaged the scaffolds using microCT on the day of implantation.

REPORTABLE OUTCOMES

Manuscripts

Day DE, Jung S. Evaluation of three-dimensional scaffolds made from 13-93 and 45S5 bioactive glass fibers after in vivo implantation in rats. Proceedings of 8th Pacific Rim Conference on Ceramics and Glass Technology, Vancouver, BC, Canada (2009). In press.

Fu Q, Rahaman MN, Brown RF, Bal BS. Preparation and in vitro evaluation of bioactive glass (13-93) scaffolds with oriented microstructures for repair and regeneration of load-bearing bones. *J Biomed Mater Res Part A* (2009). In press.

Fu Q, Rahaman MN, Bal BS, Kuroki K, Brown RF. In vivo evaluation of 13-93 bioactive glass scaffolds with trabecular and oriented microstructures in a subcutaneous rat implantation model. *J Biomed Mater Res Part A* (submitted).

Modglin V, Brown RF, Fu Q, Rahaman MN, Jung S, Day DE. Assessment of *in vitro* growth and differentiation of MLO-A5 postosteoblast/preosteocyte-like cells on 13-93 porous bioactive glass scaffolds. *Acta Biomaterialia* (submitted).

Rahaman MN, Fu Q, Bal BS, Day DE, Fu H. Bioactive glass for bone and joint repair. Proceedings of 8th Pacific Rim Conference on Ceramics and Glass Technology, Vancouver, BC, Canada (2009). In press.

Presentations

Day DE, Jung S. Evaluation of three-dimensional scaffolds made from 13-93 and 45S5 bioactive glass fibers after in-vivo implantation in rats. Invited Presentation, 8th Pacific Rim Conference on Ceramics and Glass Technology, Vancouver, BC, Canada, May 31-June 5, 2009.

Modglin V, Brown RF, Fu Q, Rahaman MN. Growth and function of MLO-A5 cells on 13-93 glass trabecular scaffolds. Poster presentation, Society for Biomaterials Annual Meeting, San Antonio, TX, April, 2009.

Modglin V, Brown RF, Jung S, Day DE. Performance of 13-93 glass fiber scaffolds with osteogenic cells. Poster presentation, Society for Biomaterials Annual Meeting, San Antonio, TX, April, 2009.

Rahaman MN. Bioactive glass for bone and joint repair. Invited Presentation, 8th Pacific Rim Conference on Ceramics and Glass Technology, Vancouver, BC, Canada, May 31-June 5, 2009.

Degrees Obtained which were Supported by this Award

Fu Q. Doctor of Philosophy in Ceramic Engineering. Thesis: 'Freeze Casting of Bioactive Glass and Ceramic Scaffolds for Bone Tissue Engineering'. Missouri University of Science and Technology, August, 2009.

Modglin V. Master of Science in Applied and Environmental Biology. Thesis: '*In Vitro* Evaluation of Bioactive Glass Scaffolds and Modified Bioactive Glasses with an Osteogenic Cell Line'. Missouri University of Science and Technology, July, 2009.

CONCLUSION

Porous three-dimensional scaffolds of silicate 13-93 bioactive glass with two different microstructures, referred to as 'fibrous' and 'trabecular', support the proliferation and differentiation of osteogenic cells. The results of *in vitro* cytotoxicity testing, cell proliferation, and cell function show that the borosilicate 13-93B1 glass has reduced biocompatibility compared to 13-93 glass, while the borate 13-93B3 compositions is clearly cytotoxic. The more rapid conversion of the 13-93B3 and 13-93B1 glasses to a hydroxyapatite-type material in a simulated body fluid leads to limited retention of strength. The 13-93 scaffolds appear to be potentially useful for bone tissue engineering applications. *In vivo* implantation in subcutaneous pockets in the dorsum of rats showed that fibrous and trabecular scaffolds of all three glasses (13-93, 13-93B1, and 13-93B3) supported abundant tissue infiltration into the scaffolds within 4 to 6 weeks.

REFERENCES

Davis DH, Giannoulis CS, Johnson RW, Desai TA (2002). Immobilization of RGD to silicon surfaces for enhanced cell adhesion and proliferation. *Biomaterials* 23:4019-27.

Fu Q, Rahaman MN, Brown RF, Bal BS, Day DE (2008). Mechanical and in vitro evaluation of 13-93 bioactive glass scaffolds prepared using a polymer foam replication technique. *Acta Biomater* 4:1854–1864.

Huang W, Day DE, Kittiratanapiboon K, Rahaman MN (2006). Kinetics and mechanisms of the conversion of silicate (45S5), borate, and borosilicate glasses to hydroxyapatite in dilute phosphate solutions. *J Mater Sci Mater Med* 17:583–596.

Kato Y, Boskey A, Spevak L, Dallas M, Hori M, Bonewald LF (2001). Establishment of an osteoid preosteocyte-like cell MLO-A5 that spontaneously mineralizes in culture. *J Bone Min Res* 16:1622–33.

Kokubo T, Kushitani H, Sakka S, Kitsugi T, Yamamuro T (1990). Solutions able to reproduce in vivo surface-structure changes in bioactive glass-ceramic A-W. *J Biomed Mater Res* 24:721–734.

Rucker M, Laschke MW, Junker D, Carvalho C, Schramm A, Mulhaupt R, Gellrich N, Menger MD (2006). Angiogenic and inflammatory response to biodegradable scaffolds in dorsal skinfold chambers of mice. Biomaterials 27:5027–38.

Sabokar A, Millett PJ, Myer B, Rushton N (1994). A rapid, quantitative assay for measurine alkaline phosphatase in osteoblastic cells *in vitro*. *Bone Miner* 27:57–67.